http://dx.doi.org/10.1016/j.apenergy.2023.122000

Investigation on overall energy performance of a novel multi-functional PV/T window

Chuyao Wang [1 *], Hongxing Yang [1 *], Jie Ji [2].

[1]Renewable Energy Research Group (RERG), Department of Building Environment and Energy Engineering, The Hong Kong Polytechnic University, Hong Kong, China

[2]Department of Thermal Science and Energy Engineering, University of Science and Technology of China, Hefei, China

Abstract

PV windows are considered to be a promising building-integrated PV technology due to their excellent electrical, daylighting and thermal performance. However, the shading of the PV cells increases the heating load in winter and the high temperature of PV cells exacerbates the cooling load in summer. Moreover, a significant portion of the heat absorbed by the PV modules is usually wasted. To address these issues, this paper proposed a multi-functional PV/T window. This system could recover the heat on PV cells for producing warm air in winter and hot water in other seasons. As a result, the proposed system can realize the combined PV/T utilization of solar energy and reduce the seasonal thermal needs of the building. First, the mathematical model of the proposed window was developed and validated. Next, the developed model was integrated into building energy software to evaluate the overall energy performance of the proposed window in four different cities of Yangtze River region: Shanghai, Nanjing, Wuhan, and Chongqing in China. These cities experience the subtropical humid climate (Cfa in the Köppen-Geiger classification) and belong to the zones with medium global horizontal irradiation. The sensitivity analysis revealed that the optimal slat angles are between 0° and 40°, while the optimal orientation angles range from 30° to 60°. Selecting low-iron glass as the inner glass resulted in the lowest overall energy consumption. By adopting the MFPV/T window, the annual operation cost of the studied case could be reduced by 34% (6.4 \$/m^2), 36% (7.0 \$/m^2), 28% (5.7 \$/m^2), and 16% (2.9 \$/m^2) in these four cites, respectively. Additionally, the annual CO_2 emissions could be curtailed by 53.5, 58.5, 47, and 22.3 kg/m^2, respectively.

Keywords: Double-skin window; PV/T; Yangtze River region; Building energy saving; Sensitivity analysis.

Nomenclature

Abbreviation

MFPV/T Multifunctional photovoltaic/thermal

GHI Global horizontal irradiation

Symbol

A area (m^2)

C heat capacity (J/kgK)

D thickness (m)

E power generation (W/m^2)

g the gravity constant (m/s^2)

h heat transfer coefficient (W/m^2K)

H height of the cavity (m)

I absorbed solar radiation (W/m^2)

Nu Nusselt number

Pr Prandtl number

Ra Rayleigh number

sw blind width (m)

y ratio of blind spacing to the blind width

R reflectance rate

si blind tilt angle (rad)

hs projected sun altitude angle (rad)

F view factor

J radiant intensity (W/m^2)

G incident solar radiation (W/m^2)

T temperature (K)

N node number in the vertical direction

M node number in the horizontal direction

v airflow rate (m/s)

ρ density (kg/m^3)

σ Stefan-Boltzman's constant (W/m^2K^4)

τ transmittance

ς emissivity

λ thermal conductivity (W/mK)

ϕ latitude angle (rad)

γ azimuth angle (rad)

ψ inclination angle (rad)

τ transmittance

Br temperature coefficient (K^{-1})

U equivalent heat transfer coefficient

η_0 PV efficiency

Subscript

a cavity air

d diffusive irradiation

b beam irradiation

c convection heat transfer

r radiative heat transfer

g, o outer glazing

g, i inner glazing

p copper pipe

w water

b back side of blind

f front side of blind

1

1. Introduction

Building-related carbon emissions represent a significant portion of global energy-related carbon emissions with 28% resulting from building energy consumption, including appliances, natural gas, heating, and cooling [1]. Integration of solar energy into building envelopes can effectively reduce building energy consumption, making it an important approach towards international carbon neutrality [2]. Windows occupy a large proportion of the building envelope in modern office buildings. Statistics from the U.S. Department of Energy state that windows contribute to around 43% of building end energy use [3]. The integration of PV technology and windows, known as PV windows, can realize the functions of thermal insulation, daylighting, ventilation, and outdoor view while generating clean electricity [4]. Thus, this technology plays an increasingly important role in the field of building energy efficiency. To date, a great deal of research has been conducted on PV windows.

1.1 Related works and research gap

Semi-Transparent PV (STPV) glazing is a popular component for constructing the PV windows [5], in which the PV cells are laminated in a sandwich structure between two glass sheets. The PV cells used STPV glazing mainly include c-Si cells, thin-film cells, organic PV cells, and dye-sensitized solar cells, etc [6]. This type PV window are classified according to their structure as single-glazed, double-glazed, and vacuum windows [7]. Several researchers, such as Olivieri et al [8], Skandalos et al [9], Alrashidi et al [10], and Yoon et al [11], tested the thermal and electrical performance of the single-glazed PV windows integrated with a-Si cells, CdTe cells, c-Si cells, and dye sensitization cells. The power generation performance tests were conducted at different PV capacities, and the comparison with ordinary glass showed that the heat gain in the room was reduced significantly. Lu et al [12], Fang et al [13], Xu et al [14] investigated the energy consumption of the buildings installed with the single-glazed PV windows. It was found that the building energy performance could be improved, especially in cooling-dominant areas.

Since single-glazed PV window cannot meet the insulation needs of buildings, double-glazed PV window is proposed by attaching a layer of glass behind the STPV glazing. The double-glazed PV

windows are currently the most widely studied and used system due to their low cost and simple structure [15]. In the past, numerous studies on the double-glazed PV windows are conducted in terms of electrical [16-18], thermal [19-21] and daylight performance [22, 23]. For instance, Wang et al. [24] evaluated the energy saving performance of the double-skin a-Si window in Hong Kong. Chen et al [25] conducted a numerical evaluation of the double-skin c-Si window in southwest China. The parameter such as air gap depth, PV coverage ratio, were optimized to maximum energy saving potential. Sun et al. [26] investigated the energy and daylight performance of double-skin CdTe window in China, and the factors regarding window design were determined in different area.

The PV vacuum window is a new technology developed in recent years, which is constructed by replacing the back sheet of double-skin PV window with the vacuum glazing. Therefore, the thermal insulation performance is greatly improved. Qiu et al. [27] studied the daylighting and energy performance of the a-Si vacuum window. They concluded that the visual comfort could be enhanced while the building energy consumption was reduced. Ghosh et al. [28] studied the thermal and electrical performance of the c-Si vacuum window. Then, the thermal [29] and visual [30] comfort of this window were also evaluated. Ji et al. [31] investigated the overall energy-saving performance of the CdTe vacuum window. The results showed that the energy saving performance exists in all kinds of climate regions in China.

Integrating PV modules with shading devices such as PV blinds is another approach to constructing PV windows. This novel structure could can bring more flexible control on the daylighting, thermal and electrical performance of the PV window. Luo et al. [32] proposed a double-skin window with PV blind. They found that this PV window exhibits the better thermal performance compared with conventional double-skin PV window. Kang et al. [33] conducted a theoretical analysis of the PV blinds in double-skin window. The effect of blin size and tilt angle on electrical performance were analyzed. Gao et al [34] proposed a PV window with sun-tracking blind. The electrical and daylighting performance under different sun-tracking method were compared. Hong et al. [35] developed a control method of the PV blind. Then, the corresponding experimental results indicated that the lighting and air-conditioning consumption was reduced when using this control method [36].

Numerous experimental and simulation studies have shown that replacing conventional windows

with PV windows can significantly reduce the net energy consumption of buildings [37]. However, some research gaps still exist. Firstly, in cooling seasons, the high temperature of PV cells may increase the building's cooling load and reduce electrical efficiency. Although some researchers, such as Peng et al [38], Luo et al [39], and Chialastri et al [40], proposed the ventilation double-skin window to exhaust waste heat on PV modules, the cooling effect is still limited due to the poor heat exchange of air. Additionally, the heat on the PV modules is usually released into the environment with the ventilation air. As a result, the comprehensive utilization ratio of solar energy on the window is low. Secondly, in heating seasons, the indoor heat gain is reduced due to the shading effect of PV cells, leading to an increase in the building heating load. Wang et al [41] and Jia et al [42] used the ventilation air of PV windows to recover a part of the heat on PV glazing. However, the comprehensive utilization ratio of solar energy and indoor heat gain remain poor because the PV glazing is directly exposed to cold air, causing significant heat loss. [43].

1.2 Novelty and contribution

The research gaps described above imply that the current PV windows suffer mainly from low solar energy utilization and poor seasonal adaptability. These issues are especially pronounced in the Yangtze River region, characterized by significant shifts in weather conditions [44]. This region, experiencing temperatures ranging from -5°C in winter to 40°C in summer, encounters both heating and cooling demands throughout the year. It’s noteworthy that building energy consumption contributes to 22% of China’s total carbon emissions [45]. Moreover, the Yangtze River region accounts for 45.1 % of China’s gross domestic product, resulting in a national carbon emission of 35.8% [46]. Consequently, the development of PV windows with high solar energy utilization and seasonal adaptability is essential to reduce building energy consumption in the Yangtze River region, playing a crucial role in achieving China’s carbon peaking and carbon neutrality goals. Guo et al. [47] and Xu et al. [43] respectively proposed the reversible windows for the Yangtze River region to increase the indoor heat gain in winter. However, the solar energy utilization and the reduction of heat gain in summer were still not improved.

In order to solve the aforementioned problems of the PV windows, this paper proposed a novel multi-functional PV/T (MFPV/T) window. This window features a PV blind positioned within the cavity of a double-skin ventilation window. In winter, the PV blind is cooled by indoor air. The heating performance and solar energy utilization are improved, because the PV modules are placed in the middle of the window and the heat loss is reduced. In summer, the PV blind is cooled by water, leading to a significant reduction in both the temperature of the PV cells and indoor heat gain, as water provides better heat exchange than air. Furthermore, the heat on the PV blind is recovered to produce hot water.

The content of this article was organized as follows: In Section 2, the structure of the investigated window system was introduced and its mathematical model was described in detail. In Section 3, the developed model of the MFPV/T window was validated. In Section 4, the prediction methodology of the energy consumption was introduced, including lighting, PV output, air condition, and hot water. In Section 5, the sensitivity analysis of slat angle, orientation, and inner glass of the proposed window system was analyzed. Then, the overall energy performance of the MFPV/T and clear windows was compared.

2. System description

2.1. Structure and working principle

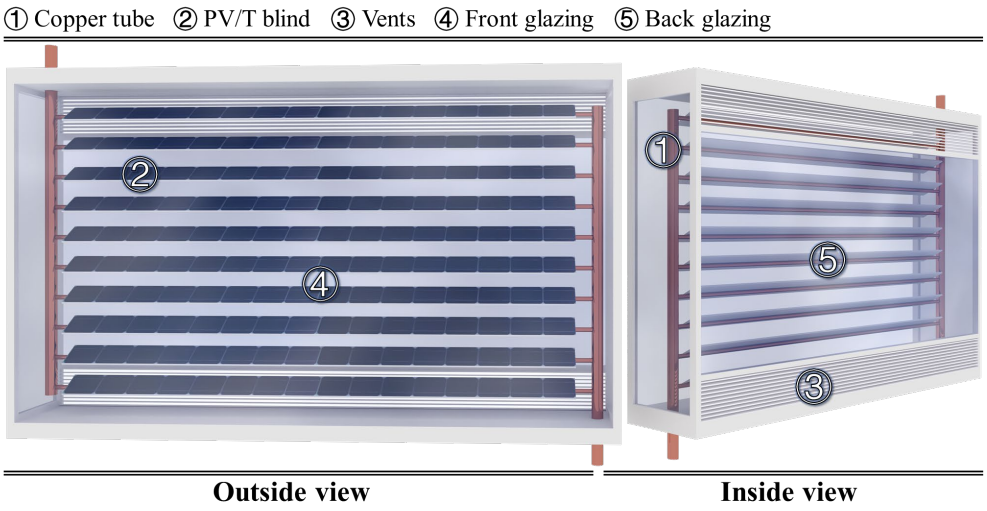

Fig. 1 The structure and main components of the proposed window system

Fig. 1 depicts the appearances of the proposed window from inside and outside views. The system comprises three layers: front glazing, back glazing, and middle PV/T blind. The front glazing is typically fabricated with ultra-clear glass to allow for increased solar energy absorption and improved efficiency. The choice of inner glass can be customized based on specific indoor environment requirements such as daylight or thermal/sound insulation. There are two vents existing on the bottom and top of the back glazing for connecting the cavity air and indoor air. The PV/T blind is the core component of the proposed window, which is a composite of PV cells, aluminum slats, and copper water pipes. The copper water pipes are welded onto the back side of the aluminum slats, and the PV cells are laminated onto the front side. The left and right ends of all copper pipes are connected to the inlet and outlet header pipes respectively. The manufacture process of the PV/T blind is similar to that of the solar PV/T collector.

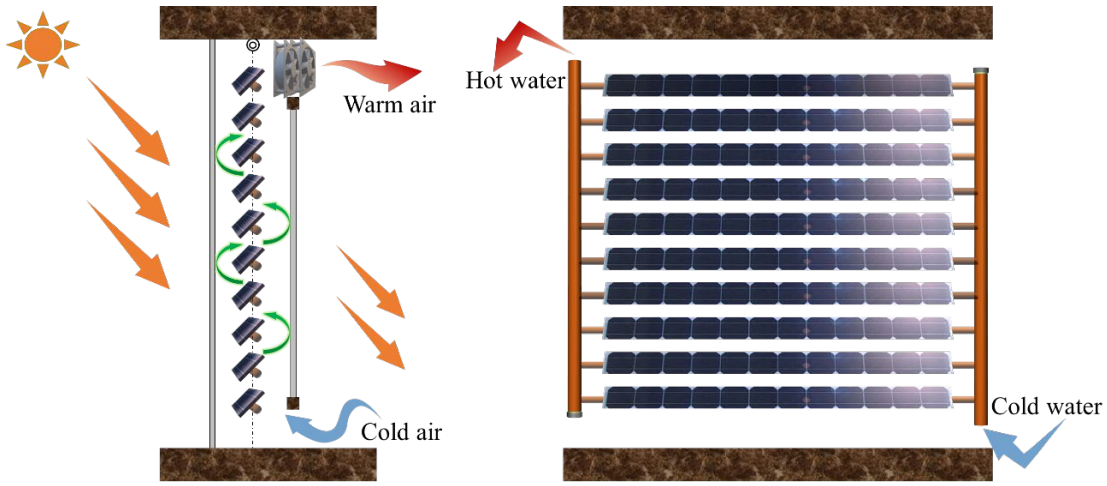

(a) PV/air mode **(b) PV/water mode**

Fig. 2 The working principle of the proposed window system

Fig. 2 depicts the working principle of the proposed window, and the work modes of the proposed system include PV/air and PV/water modes. In heating seasons, the PV/air mode is adopted. The water in the copper pipe is drained, the vents are opened, and the fans are activated. The irradiation absorbed by the PV/T blind is partly converted into clean electricity and partly into heat. Driven by the fans, the indoor air enters the cavity and is heated by flowing through the blinds, before returning

to the room. As a result, the PV efficiency increases and the indoor heating load is reduced. In non-heating seasons, the PV/water mode is adopted. The vents are closed and the fans are turned off. Driven by the water pump, the water flows through the copper pipe, absorbs heat on the PV blind, and then flows out from the outlet. This mode not only increases the PV efficiency but also reduces the indoor cooling load in summer, while producing additional domestic hot water. The proposed system achieves comprehensive solar utilization of heat and electricity in different seasons, surpassing conventional PV glass or PV blind windows by meeting the seasonal thermal demand of the building.

2.2. Mathematical Models

The operation of the proposed window is a multi-physical process that involves solar absorbance and transmittance, thermal transfer, and power generation. To simulate this system, the absorption of solar radiation on the multi-layer window is initially determined and then fed into the heat transfer and PV electricity models of the system. This section describes the mathematical models of the proposed window in terms of these two aspects. Several reasonable assumptions were made to simplify the model: (a) all thermal properties such as density, heat capacity, and thermal conductivity are considered to be constants; (b) the temperature of air and water changes only along the flow direction; (c) the irradiation reflected by the blinds is considered to be purely diffuse; and (d) the temperature of the glass and blind is uniform in the thickness direction due to their small thickness.

2.2.1. Solar absorbance and transmittance

This subsection firstly introduces the optical behavior of the blinds, which constitutes the main complexity of solar absorbance and transmittance. The PV blinds receive radiation from two sources: the outside and the inside. The outside radiation comprises irradiation directly entering through the outer glass and irradiation reflected by the outer glass, while the inside irradiation is the irradiation reflected from the inner glass. As shown in Fig. 3, the interaction of the outside irradiation in the blind cavity depends on the solar altitude angle. If the projected solar altitude angle exceeds the critical

angle, no beam radiation can penetrate the blinds, and the lower area of the blinds receives beam radiation. Conversely, when the projected solar altitude angle is lower than the critical angle, a part of the beam radiation passes through the blinds, and the front side of the blinds can receive beam radiation entirely.

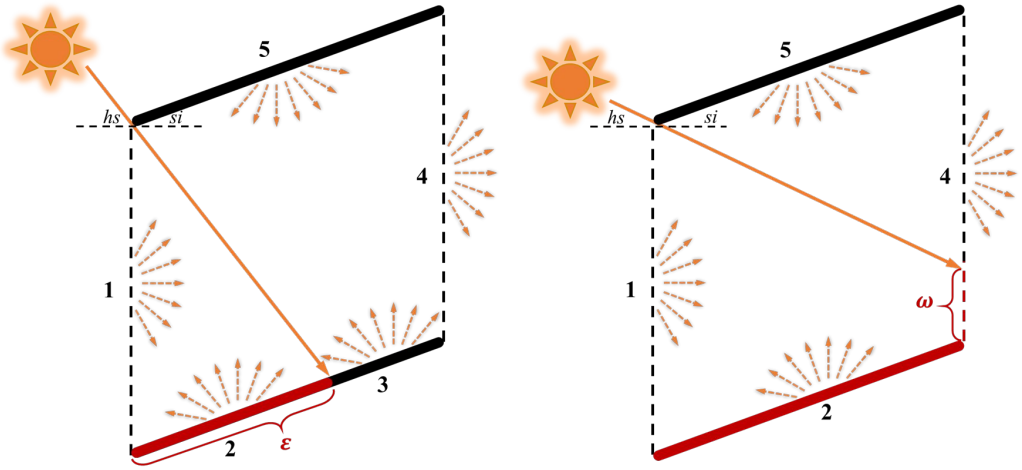

Fig. 3 Schematic of the interaction of the outside irradiation in the blind cavity

As shown in Fig. 3, *si* represents the slat angle of blind which varies between 0° and 90°. *hs* represents the projected solar altitude angle. It is calculated by [48]:

$$hs = arctan\left(\frac{sin\,(\phi)}{cos\,(\gamma_{sun}-\gamma_g)cos\,(\phi)}\right) \tag{1}$$

where, ϕ is the solar altitude angle. γ_{sun} and γ_g respectively represent the azimuth of the sun and windows.

The critical angle is calculated by:

$$\theta = arctan\left(\frac{y-sin\,(si)}{cos\,(si)}\right) \tag{2}$$

where, *y* is the ratio of the blind spacing to the blind width.

In the Fig. 3, ε is the proportion of the unshaded blind and ω is the proportion of the penetrating beam radiation through the blind. They are calculated by:

$$\begin{cases} \varepsilon = 1 \\ \omega = 1 - \dfrac{(sin(si)+cos\,(si)tan\,(hs))}{y}, \; hs < \theta \end{cases} \tag{3}$$

$$\begin{cases} \varepsilon = \dfrac{y}{sin(si)+cos\,(si)tan\,(hs)}, & hs \geq \theta \\ \omega = 0 \end{cases} \tag{4}$$

The interaction of diffusive irradiation in blind cavity was calculated by the radiosity method. As shown in Fig. 3, the surfaces of the blind cavity are divided into five parts. The surface 1 is the irradiation inlet and the surface 4 is the irradiation outlet. The surface 2 and surface 3 are respectively the unshaded and shaded parts of the blind front side. The surface 5 is the blind back side. The radiosity equation set of all surfaces is written as:

$$\begin{cases} J_1 = G_{d,v}^{+} \\ J_2 = (G_{b,t}^{+} + J_1 y F_{1-2} + J_4 y F_{4-2} + J_5 F_{5-2}) R_f \\ J_4 = 0 \\ J_5 = (J_1 y F_{1-5} + J_2 F_{2-5} + J_4 y F_{4-5}) R_b \end{cases}, \; hs < \theta \tag{5}$$

$$\begin{cases} J_1 = G_{d,v}^{+} \\ J_2 \varepsilon = (G_{b,t}^{+} \varepsilon + J_1 y F_{1-2} + J_4 y F_{4-2} + J_5 F_{5-2}) R_f \\ J_3 (1-\varepsilon) = (J_1 y F_{1-3} + J_4 y F_{4-3} + J_5 F_{5-3}) R_f \\ J_4 = 0 \\ J_5 = (J_1 y F_{1-5} + J_2 \varepsilon F_{2-5} + J_3 (1-\varepsilon) F_{3-5} + J_4 y F_{4-5}) R_b \end{cases}, \; hs \geq \theta \tag{6}$$

where, $G_{d,v}^{+}$ is the diffusive irradiation on the outside vertical plane and $G_{b,t}^{+}$ is the outside beam irradiation on the blind tilt surface. R_f and R_b represent the blind reflectance of the front and back sides. *F* denotes the view factor between two surfaces.

After obtaining the radiosity on the surfaces of blind cavity, the blind transmittance, absorbance, and reflectance when receiving outside irradiation are calculated by:

$$\tau_{b-b}^{+} = \omega \tag{7}$$

$$\tau_{b-d}^{+} = \frac{J_1 y F_{1-4} + J_2 \varepsilon F_{2-4} + J_3 (1-\varepsilon) F_{3-4} + J_5 F_{5-4}}{y}, G_{d,v}^{+} = 0 \;\&\; G_{b,v}^{+} = 1 \tag{8}$$

$$\tau_{d-d}^{+} = \frac{J_1 y F_{1-4} + J_2 \varepsilon F_{2-4} + J_3 (1-\varepsilon) F_{3-4} + J_5 F_{5-4}}{y}, G_{d,v}^{+} = 1 \;\&\; G_{b,v}^{+} = 0 \tag{9}$$

$$\alpha_b^{+} = \left(J_2 \varepsilon + J_3 (1-\varepsilon)\right)\left(\frac{1}{R_f} - 1\right) + J_5 \left(\frac{1}{R_b} - 1\right), G_{d,v}^{+} = 0 \;\&\; G_{b,v}^{+} = 1 \tag{10}$$

$$\alpha_d^{+} = \left(J_2 \varepsilon + J_3 (1-\varepsilon)\right)\left(\frac{1}{R_f} - 1\right) + J_5 \left(\frac{1}{R_b} - 1\right), G_{d,v}^{+} = 1 \;\&\; G_{b,v}^{+} = 0 \tag{11}$$

$$\gamma_b^{+} = \frac{J_2 \varepsilon F_{2-1} + J_3 (1-\varepsilon) F_{3-1} + J_5 F_{5-1}}{y}, G_{d,v}^{+} = 0 \;\&\; G_{b,v}^{+} = 1 \tag{12}$$

$$\gamma_b^{+} = \frac{J_2 \varepsilon F_{2-1} + J_3 (1-\varepsilon) F_{3-1} + J_5 F_{5-1}}{y}, G_{d,v}^{+} = 1 \;\&\; G_{b,v}^{+} = 0 \tag{13}$$

where, τ, α and γ respectively represent transmittance, absorbance, and reflectance. $G_{b,v}^{+}$ is the

beam irradiation on the vertical plane. Subscript *b* and *d* respectively represent beam and diffuse irradiation. *b*-*b*, *b*-*d*, and *d*-*d* are beam to beam, beam to diffuse, and diffuse to diffuse irradiation.

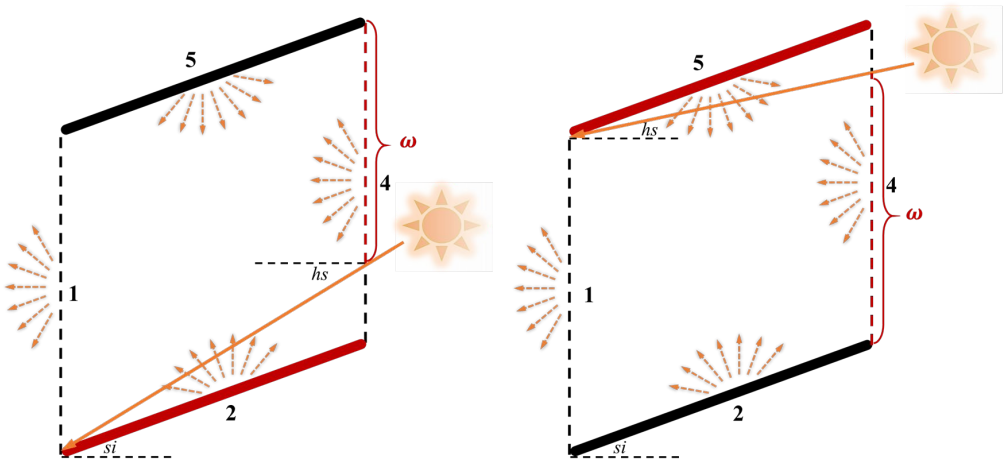

Fig. 4 Schematic of the interaction of the inside irradiation in the blind cavity

The interaction of the inside irradiation is shown in Fig. 4. It can be deduced from basic geometric principles that the projected solar altitude angle of the inside beam irradiation is less than the inside critical angle. Consequently, it can be inferred that the beam irradiation emanating from the inner glass is capable of passing through the blind. Furthermore, the interaction of inside irradiation within the blind cavity is categorized into two scenarios, as illustrated in Fig. 4. When hs is larger than the slat angle, the front side of the blinds fully receives the beam radiation. Conversely, when hs is smaller than the slat angle, the back side of the blinds receives the entire beam radiation. The proportion of the penetrating beam radiation through the blind is calculated by:

$$\omega = \begin{cases} y - \sin(si) + co\,s(si)\,ta\,n(hs), & hs < si \\ y - co\,s(si)\,ta\,n(hs) + \sin(si), & hs \geq si \end{cases} \tag{14}$$

When calculating the diffusive irradiation, the surfaces of the blind cavity are divided into four parts. The radiosity equation set of all surfaces is written as:

$$\begin{cases} J_1 = 0 \\ J_2 = (J_1 y F_{1-2} + J_4 y F_{4-2} + J_5 F_{5-2}) R_f \\ J_4 = G_{d,v}^- \\ J_5 = (G_{b,t}^- + J_1 y F_{1-5} + J_2 F_{2-5} + J_4 y F_{4-5}) R_b \end{cases}, \quad hs < si \tag{15}$$

$$\begin{cases} J_1 = 0 \\ J_2 = (G_{b,t}^- + J_1 yF_{1-2} + J_4 yF_{4-2} + J_5 F_{5-2})R_f \\ J_4 = G_{d,v}^- \\ J_5 = (J_1 yF_{1-5} + J_2 F_{2-5} + J_4 yF_{4-5})R_b \end{cases}, \ hs \geq si \tag{16}$$

where, $G_{d,v}^-$ is the diffusive irradiation on the inside vertical plane and $G_{b,t}^-$ is the inside beam irradiation on the blind tilt surface.

Similarly, the blind transmittance, absorbance, and reflectance the when receiving inside irradiation are calculated by:

$$\tau_{b-b}^- = \omega \tag{17}$$

$$\tau_{b-d}^- = \frac{J_4 yF_{4-1} + J_2 F_{2-1} + J_5 F_{5-1}}{y}, G_{d,v}^- = 0 \ \& \ G_{b,v}^- = 1 \tag{18}$$

$$\tau_{d-d}^- = \frac{J_4 yF_{4-1} + J_2 F_{2-1} + J_5 F_{5-1}}{y}, G_{d,v}^- = 1 \ \& \ G_{b,v}^- = 0 \tag{19}$$

$$\alpha_b^- = J_2(\frac{1}{R_f} - 1) + J_5(\frac{1}{R_b} - 1), G_{d,v}^- = 0 \ \& \ G_{b,v}^- = 1 \tag{20}$$

$$\alpha_d^- = J_2(\frac{1}{R_f} - 1) + J_5(\frac{1}{R_b} - 1), G_{d,v}^- = 1 \ \& \ G_{b,v}^- = 0 \tag{21}$$

$$\gamma_b^- = \frac{J_2 F_{2-4} + J_5 F_{5-4}}{y}, G_{d,v}^- = 0 \ \& \ G_{b,v}^- = 1 \tag{22}$$

$$\gamma_b^- = \frac{J_2 F_{2-4} + J_5 F_{5-4}}{y}, G_{d,v}^- = 1 \ \& \ G_{b,v}^- = 0 \tag{23}$$

The solar transmittance, reflectance, and absorbance of the inner and outer glass are determined using the ray-tracking technology in ISO 9050. They are respectively calculated by:

$$\tau_g = \frac{t(1-r)^2}{1-t^2 r^2} \tag{24}$$

$$\gamma_g = r[1 + \frac{t^2(1-r)^2}{1-t^2 r^2}] \tag{25}$$

$$\alpha_g = 1 - \tau - \gamma \tag{26}$$

where, t and r depend on the solar incident angle by Bouger's law and Fresnel's law.

For beam irradiation, the incident angle is calculated as [49]:

$$\cos\psi = \sin(\phi)\cos(\beta) + \cos(\phi)\cos(\beta)cos\ (\gamma_{sun} - \gamma_g) \tag{27}$$

where, β is the inclination angle of glass, 90° in this study.

For diffusive irradiation, the effective incident angle of 60° is used for calculating the solar transmittance, reflectance, and absorbance of glass [50]. This result is obtained through spherical

integration of isotropy diffuse irradiation, which is widely accepted and recognized in the field [49].

Once the optical properties of the three layers in the proposed window are determined, the solar absorbance of each layer and the overall transmittance of the system can be calculated using the net radiation method as described in reference [51]. This method accounts for the infinite reflection and absorption of both beam and diffuse radiation among the layers.

2.2.2. Heat transfer and power generation

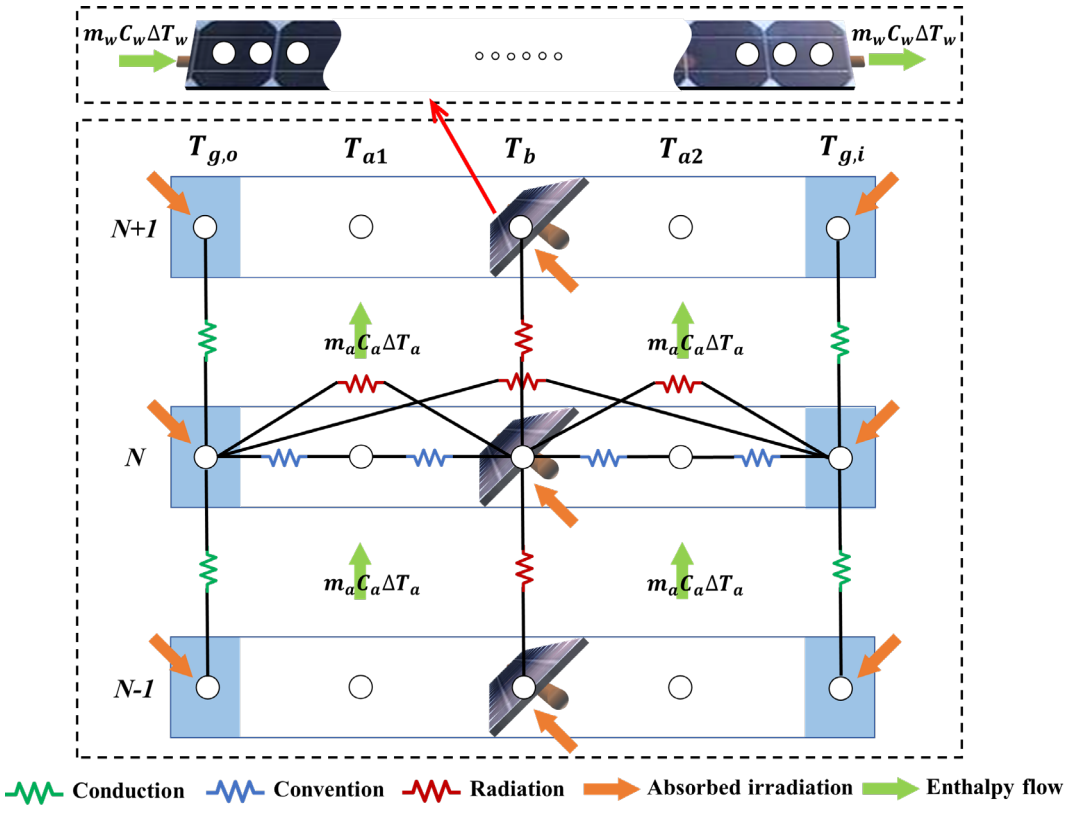

Fig. 5 The 3-D node distribution of the zonal model of the proposed window

The energy flow within the proposed window involves power generation, conduction, convention, long-wave and short-wave radiation occurring between the solider layers. In addition, the enthalpy flows of the air and water exists in vertical cavity and horizontal pipe, respectively. In this study, the zonal model is employed for simulating energy behavior of the proposed window. The 3-D node distribution of the used zonal model is shown in Fig. 5. The system includes five layers in the depth direction, namely outer glass, out air gap, blind, inner air, and inner glass. They are respectively

represented by subscript 'g,o', '$a1$', 'b', '$a2$', and 'g,i'. The blind layers are discretized in the horizontal and vertical directions while other layers are only discretized in the vertical direction. The node numbers in the vertical and horizontal directions are indicated by superscripts '*N*' and '*M*', respectively. The zonal model of the proposed window is obtained by applying the energy balance equation to nodes.

The energy balance of outer glass includes the terms of conduction, long-wave radiation, and solar absorbance. The equation is written as:

$$(D\rho C)_{g,o}\frac{\partial T_{g,o}^{N}}{\partial t} = (D\lambda)_{g,o}\frac{T_{g,o}^{N+1}+T_{g,o}^{N-1}-2T_{g,o}^{N}}{\Delta z^{2}} + I_{g,o} + h_{r,go-e}\left(T_e - T_{g,o}^{N}\right) + h_{c,go-amb}\left(T_{amb} - T_{g,o}^{N}\right) + h_{r,go-b}\left(T_b - T_{g,o}^{N}\right) + h_{r,go-gi}\left(T_{g,i} - T_{g,o}^{N}\right) + h_{c,go-a1}\left(T_{a1} - T_{g,o}^{N}\right) \quad (28)$$

where, D and ρ represent the thickness and density while C and λ are the heat capacity and thermal conductivity. h_c, h_r are convective and radiative heat transfer coefficients. I is the irradiation absorbed by the components. Δz is the distance between nodes in vertical direction.

Similar with outer glass, the equation of inner glass is written as:

$$(D\rho C)_{g,i}\frac{\partial T_{g,i}^{N}}{\partial t} = (D\lambda)_{g,i}\frac{T_{g,i}^{N+1}+T_{g,i}^{N-1}-2T_{g,i}^{N}}{\Delta z^{2}} + I_{g,i} + (h_{c,gi-room} + h_{r,gi-room})\left(T_{room} - T_{g,i}^{N}\right) + h_{r,gi-b}\left(T_b - T_{g,i}^{N}\right) + h_{r,go-gi}\left(T_{g,o} - T_{g,i}^{N}\right) + h_{c,gi-a2}\left(T_{a2} - T_{g,i}^{N}\right) \quad (29)$$

The energy balance of air gap only includes the terms of convention and enthalpy flow. The equations are written as:

$$(D\rho C)_{a1}\frac{\partial T_{a1}^{N}}{\partial t} = h_{c,go-a1}\left(T_{g,o} - T_{a1}^{N}\right) + h_{c,b-a}(T_b - T_{a1}^{N}) - v_a(D\rho C)_{a1}\frac{T_{a1}^{N-1}-T_{a1}^{N}}{\Delta z} \quad (30)$$

$$(D\rho C)_{a2}\frac{\partial T_{a2}^{N}}{\partial t} = h_{c,gi-a2}\left(T_{g,i} - T_{a2}^{N}\right) + h_{c,b-a}(T_b - T_{a2}^{N}) - v_a(D\rho C)_{a2}\frac{T_{a2}^{N-1}-T_{a2}^{N}}{\Delta z} \quad (31)$$

where, v_a is the air flow rate.

The energy balance of PV blind is relatively complicated due to 3-dimensional heat transfer. It includes the terms of conduction, convention, long-wave radiation, solar absorbance, and power generation. The equation is written as:

For PV/air mode, the heat transfer of copper pipes is not considered due to the small thermal mass and fin efficiency [52]:

$$(D\rho C)_b \frac{\partial T_b^{N,M}}{\partial t} = I_b + h_{r,go-b}\left(T_{g,o} - T_b\right) + h_{c,b-a}(T_{a1} - T_b) + h_{c,b-a}(T_{a2} - T_b) + h_{r,gi-b}\left(T_{gi} - T_b\right) + h_{r,b-b}\left(T_b^{N+1,M} + T_b^{N-1,M} - 2T_b^{N,M}\right) + (D\lambda)_b \frac{T_b^{N,M+1} + T_b^{N,M-1} - 2T_b^{N,M}}{\Delta y^2} - E \quad (32)$$

For PV/water mode:

$$(D\rho C)_b \frac{\partial T_b^{N,M}}{\partial t} = I_b + h_{r,go-b}\left(T_{g,o} - T_b\right) + h_{c,b-a}(T_{a1} - T_b) + h_{c,b-a}(T_{a2} - T_b) + h_{r,gi-b}\left(T_{gi} - T_b\right) + h_{r,b-b}\left(T_b^{N+1,M} + T_b^{N-1,M} - 2T_b^{N,M}\right) + (D\lambda)_b \frac{T_b^{N,M+1} + T_b^{N,M-1} - 2T_b^{N,M}}{\Delta y^2} + U(T_p^{N,M} - T_b^{N,M}) - E \quad (33)$$

where, Δy is the distance between nodes in horizontal direction. U is the equivalent heat transfer coefficient between copper pipe and blind.

The power generation of the PV blind is calculated as:

$$E = G_{total,t}\eta_0[1 - Br(T_b - 298.15)] \quad (34)$$

where, $G_{total,t}$ is the total irradiation incident on the front side of PV blind; η_0 is the standard PV efficiency; *Br* is the temperature coefficient of PV cells.

The energy balance of copper pipe only occurs in PV/air mode. The equation is written as:

$$\pi d_w(\rho CD)_p \frac{\partial T_p^{N,M}}{\partial t} = \pi d_w(\lambda D)_p \frac{T_p^{N,M+1} + T_p^{N,M-1} - 2T_p^{N,M}}{\Delta y^2} + \pi d_w h_{c,p-w}\left(T_w^{N,M} - T_p^{N,M}\right) + U(T_b^{N,M} - T_p^{N,M}) \quad (35)$$

where, subscript 'p' and 'w' respectively represents the copper pipe and water in pipe. d_w is the inner diameter of water pipe.

The energy balance of water in pipe includes the terms of convention, conduction, and enthalpy flow. The equation is written as:

$$\frac{d_w}{4}(\rho C)_w \frac{\partial T_w^{N,M}}{\partial t} = \frac{d_w}{4}\lambda_w \frac{T_w^{N,M+1} + T_w^{N,M-1} - 2T_w^{N,M}}{\Delta y^2} - \frac{d_w}{4}\rho_w v_w C_w \frac{T_w^{N,M-1} - T_w^{N,M}}{\Delta y} + h_{c,w-p}(T_p^{N,M} - T_w^{N,M}) \quad (36)$$

where, v_w is the water flow rate.

The convective heat transfer coefficient between outer glass and outdoor air is related to the wind speed v_{amb}. The equation is written as [53]:

$$h_{c,go-amb} = 5.62 + 3.9v_{amb} \tag{37}$$

The convective heat transfer coefficient between inner glass and room air depends on the temperature difference. The equation is written as [41]:

$$h_{c,room} = 2.03|T_{g,in} - T_{room}|^{1/3} \tag{38}$$

When the fan is turned on, the following equation is used to calculated the heat transfer coefficients between glass and cavity air: [54]:

$$h_{c,go/gi-a} = 5.62 + 3.9v_a \tag{39}$$

When the fan is turned off, the flow state of cavity air is natural convection. The correlation equations in ISO 15099 is employed [55]:

$$h_{c,go/gi-a} = \frac{Nu \cdot \lambda_a}{D_a} \tag{40}$$

$$Nu = (Nu_1, Nu_2)\max \tag{41}$$

$$Nu_1 = \begin{cases} 0.0673838Ra^{1/3}, Ra > 50000 \\ 0.028154Ra^{0.4134}, 500000 > Ra > 10000 \\ 1 + 1.7596678 \times 10^{-10}Ra^{2.2984755}, Ra < 10000 \end{cases} \tag{42}$$

$$Nu_2 = 0.242(\frac{Ra}{H/D_a})^{0.272} \tag{43}$$

where, Nu, Ra, and λ_a are the Nusselt number, Rayleigh number, and the air thermal conductivity; H represents the height of air cavity, respectively.

When the fan is turned off, the convective heat transfer coefficients between blind and cavity air is same as that between cavity and glass. When the fan is on, this convective coefficient was calculated by [56]:

$$h_{c,b-a} = \frac{Nu \cdot \lambda_a}{sw} \tag{44}$$

$$Nu = 0.51Re^{0.5}Pr^{0.37} \tag{45}$$

where, Re and Pr are the Reynolds and Prandtl numbers of the cavity air.

The forced convective heat transfer coefficient between water and pipe wall in copper pipe is calculated as [57]:

$$h_{c,p-w} = \frac{Nu \cdot \lambda_w}{d_w} \tag{46}$$

$$Nu = \begin{cases} 0.023 Re^{0.8} Pr^{0.4}, & \text{turbulent flow} \\ 3.66, & \text{laminar flow} \end{cases} \tag{47}$$

where, Re and Pr are the Reynolds and Prandtl numbers of the water in pipe.

The radiative heat transfer coefficients between outer glass and outdoors, between inner glass and indoors, between inner glass and outer glass, are calculated as:

$$h_{r,\mathrm{go}-e} = \varsigma_g \sigma ({T_{g,o}}^2 + {T_e}^2)(T_{g,o} + T_e) \tag{48}$$

$$h_{r,gi-room} = \varsigma_g \sigma ({T_{g,i}}^2 + {T_{room}}^2)(T_{g,i} + T_{room}) \tag{49}$$

$$h_{r,go-gi} = \frac{\sigma ({T_{g,o}}^2 + {T_{g,i}}^2)(T_{g,o} + T_{g,i})}{\frac{1}{\varsigma_{g,o}} + \frac{1}{\varsigma_{g,i}} - 1} \tag{50}$$

When the slat tilt angle is less than 90°, both the front and back side of the blinds have radiation heat exchange with the outer glass. Thus, the radiative heat transfer coefficient should be the sum of these two parts. The equation is written as:

$$h_{r,go-b} = \frac{\sigma ({T_{g,o}}^2 + {T_b}^2)(T_{g,o} + T_b)}{\frac{1}{\varsigma_{g,o}} + \frac{1}{\varsigma_{bf}} - 2 + \frac{1}{F_{g,o-bf}}} + \frac{\sigma ({T_{g,o}}^2 + {T_b}^2)(T_{g,o} + T_b)}{\frac{1}{\varsigma_{g,o}} + \frac{1}{\varsigma_{bb}} - 2 + \frac{1}{F_{g,o-bb}}} \tag{51}$$

Similarly, this coefficient between the blind and inner glass is written as:

$$h_{r,gi-b} = \frac{\sigma ({T_{g,i}}^2 + {T_b}^2)(T_{g,i} + T_b)}{\frac{1}{\varsigma_{bf}} + \frac{1}{\varsigma_{g,i}} - 2 + \frac{1}{F_{g,i-bf}}} + \frac{\sigma ({T_{g,i}}^2 + {T_b}^2)(T_{g,i} + T_b)}{\frac{1}{\varsigma_{bb}} + \frac{1}{\varsigma_{g,i}} - 2 + \frac{1}{F_{g,i-bb}}} \tag{52}$$

The radiative heat transfer coefficient between adjacent blinds is written as

$$h_{r,b-b} = \frac{\sigma ({T_b}^2 + {T_b}^2)(T_b + T_b)}{\frac{1}{\varsigma_{bb}} + \frac{1}{\varsigma_{bf}} - 2 + \frac{1}{F_{b-b}}} \tag{53}$$

where, σ is the Stefan-Boltzmann's constant; ς_{go} and ς_{gi} are the outer and inner glass emissivity coefficients, respectively; ς_{bf} and ς_{bb} are the front and back emissivity coefficients of the blind; F_{i-j} is the view factor from the surface *i* to *j*.

2.2.3. Solving method

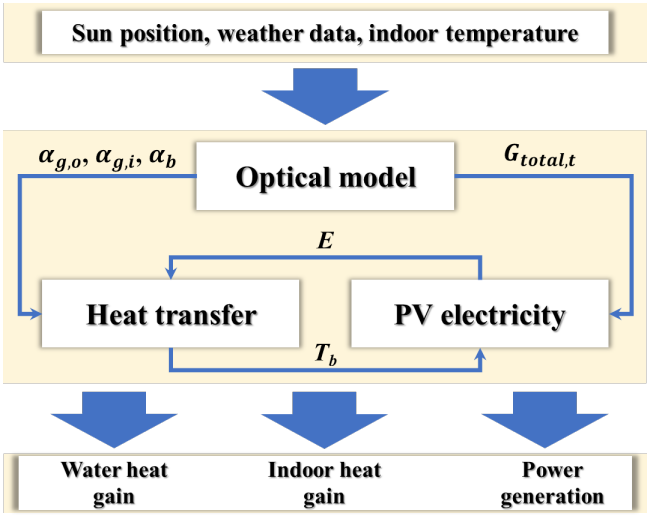

Fig. 6 The solving flowchart of the mathematical model of the proposed system

The methodology for solving the above mathematical models is depicted in Fig. 6. The input data includes the sun position, weather data, and indoor temperature, while the output data comprises the water heat gain, indoor heat gain, and power generation. To calculate the solar absorbance, solar transmittance, and the irradiation incident on the PV blind, the solar altitude angle, azimuth angle and solar radiation are entered as inputs into the optical model. The resulting solar absorbance of all components and the irradiation on the PV blind are then utilized as inputs into the heat transfer and PV electricity models, respectively. The electrical and thermal models are coupled through power generation and PV temperature and are resolved via the Jacobi iteration. Initially, the PV temperature of the heat transfer model is calculated by assuming a power generation. Subsequently, the power generation is estimated by the PV electricity model, employing the obtained PV temperature as the boundary condition. The PV temperature is then re-calculated using the heat transfer model with the new value of power generation. This iterative process is repeated until the changes in PV temperature and power fall below the residual.

3. Model validation

In this section, the proposed window's mathematical model is validated using data reported in the

reference literature. The current model, as detailed in Section 2.2, includes three components: optical behavior, heat transfer, and PV electricity. To begin the validation process, the optical model is first examined as it is relatively independent of the other models. Next, the heat transfer model is assessed by utilizing known power generation as the boundary condition, while the PV electricity model is verified using PV temperature as the boundary condition. To quantify the simulation error, the coefficient of root-mean-square error (Cv(RMSE)) and mean bias error (MBE) are employed. The equations for calculating these two metrics are given as:

$$Cv(RMSE) = \frac{\sqrt{\Sigma_{i=1}^{N}(S_i - M_i)^2/N}}{\Sigma_{i=1}^{N} M_i/N} \tag{54}$$

$$MBE = \frac{\Sigma_{i=1}^{N}(S_i - M_i)}{\Sigma_{i=1}^{N} M_i} \tag{55}$$

where, S and M represent the simulated and measured values. N is the number of the validated data. According to ASHRAE Guideline 14, the accuracy of the model is considered to be acceptable when Cv(RMSE) and MBE are lower than 30% and 10%, respectively [58].

3.1. Optical behavior

The structure of the proposed window shows that the optical behavior of this system is in agreement with that of the double-skin window with built-in blinds. Luo et al. [59] previously studied the solar transmittance of this type of windows, and their experimental data was used to validate the optical model. They conducted the sunny and cloudy experiments on July 8th and 9th, 2016 in Changsha, China. The tested system comprised two 6 mm clear glasses and a PV blind, with a blind width of 2.5 cm and a blind space of 4.5 cm, and a slat angle of 45°. The comparison between experimental and simulated results of total penetration irradiation is shown in Fig. 7. It can be found that the simulation results match the experimental results very well both on sunny and cloudy days. The Cv(RMSE)s for these two days are 8.51% and 8.36% while the MBEs are 3.19% and 5.10%. Thus, it can be concluded that the accuracy of the proposed optical model can meet the usage requirements.

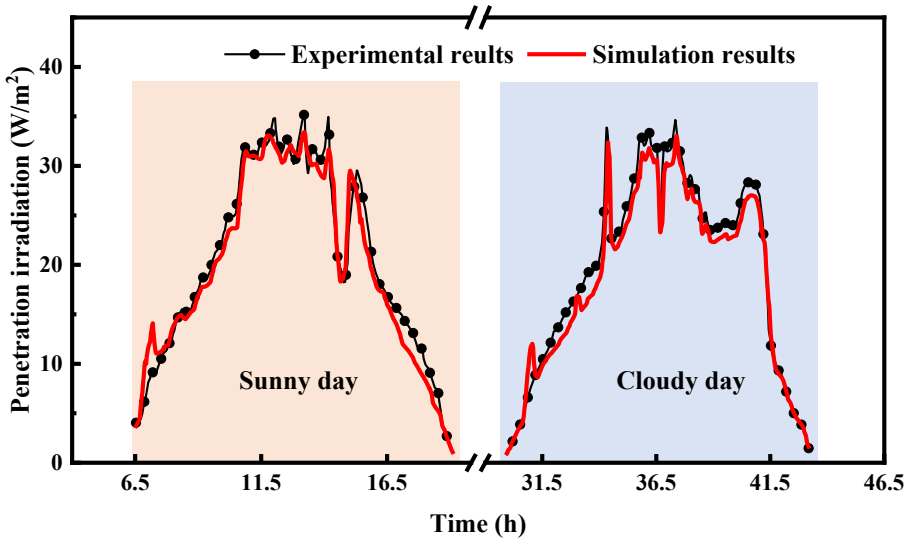

Fig. 7 The validation of the optical model

3.2. Heat transfer

When operating in the PV/air mode, the proposed system exhibits the same heat transfer characteristics as the airflow window with built-in blinds. Previous research has extensively studied this type of window. Zhang et al. [60] conducted an experiment on the airflow window with built-in blinds in two consecutive days. Details of the specific structure and physical parameters can be found in Ref [60]. The outlet air temperature and the inner glass temperature were used for validating the model. Fig. 8 displays the validation results. It can be observed that the simulated temperature agrees well with the experimental results. The error analysis reveals that the Cv(RMSE)s are 1.72% for outlet air and 1.07% for inner glass while MBEs are -0.11% for outlet air and 0.37% for inner glass. Thus, the developed model can reliably simulate the proposed window's thermal performance.

When the proposed system operates in the PV/water mode, its construction and heat transfer process are identical to those of the double glass window with pipe-embedded blinds proposed by Li et al [61]. In their study, the indoor heat gain and water heat gain of this window under the specific boundary conditions was calculated by a rigorously validated computational fluid dynamics model. In their work, the boundary conditions included an indoor temperature of 25°C, outdoor temperature of 33°C, and water inlet temperature of 25°C. The solar radiation ranged from 500 W/m^2 to 100 W/m^2. In this section, the calculated results of the developed model were compared with those in the

reference. As shown in Fig. 9, the difference in indoor and water heat gain between the developed model and the numerical model falls within the error line (10%). Thus, the model developed in this paper can accurately calculate the thermal performance of the system in PV/water mode.

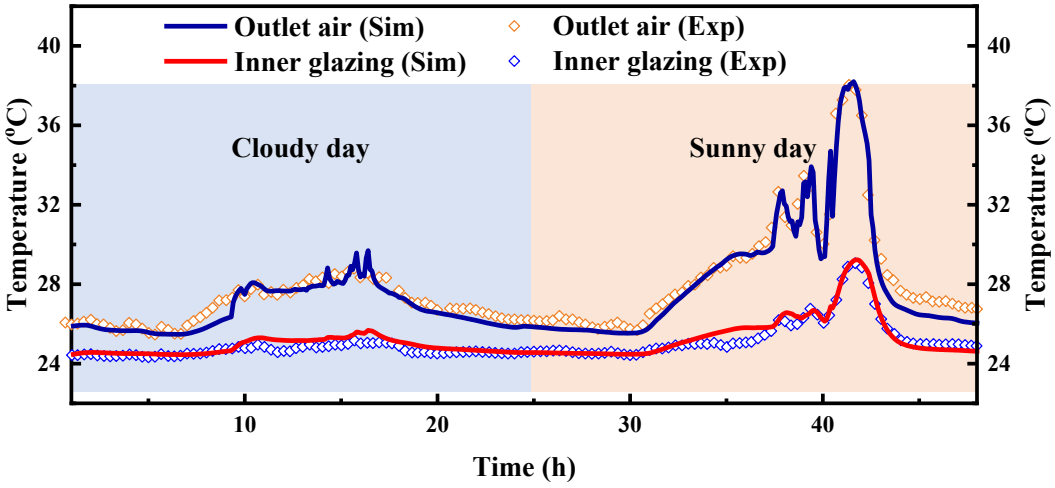

Fig. 8 The validation of the heat transfer model for air heating

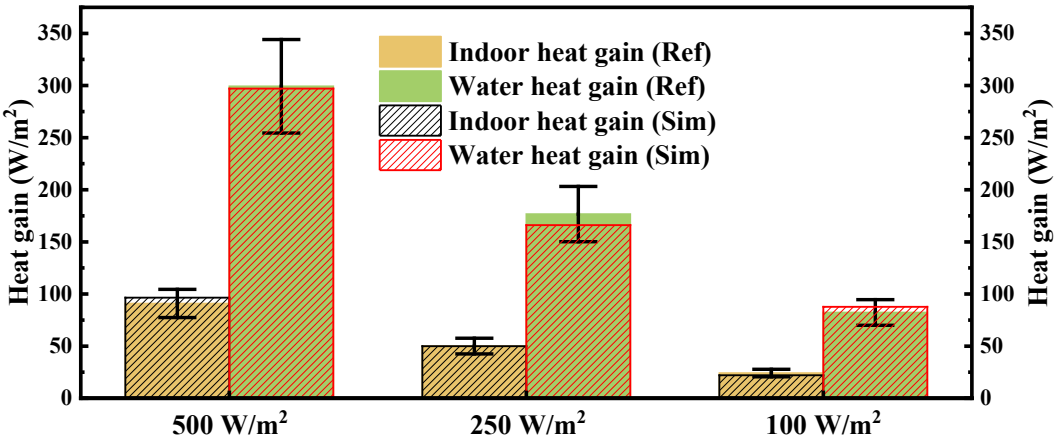

Fig. 9 The validation of the heat transfer model for water heating

3.3. PV electricity

The validity of the PV electricity model of the PV blind was assessed using the reported data by Hu et al [62]. Their study investigated a blind-integrated building facade configuration, where the PV blind was situated between the glass cover and the wall. Although the structural setup of the Trombe wall differs from the window configuration presented in this work, both systems exhibit similar power

generation characteristics. The experimental data on April 18th and 28th in Hefei, China was used to validate the PV electricity model. The slat angles in these two days were 50° and 15°, respectively. The validated optical model described in Section 2.2.1 was used to estimate the irradiation incident on the PV modules using the measured south irradiation. The calculated incident irradiation and the PV temperature obtained from the literature were then inputted into the PV electricity model. Fig. 10 shows that the simulation results and experimental data are in good agreement. The error analysis indicates that the Cv(RMSE)s are 13.62% and 12.82% while the MBEs are -4.81% and 4.56%. These errors are within the acceptable ranges.

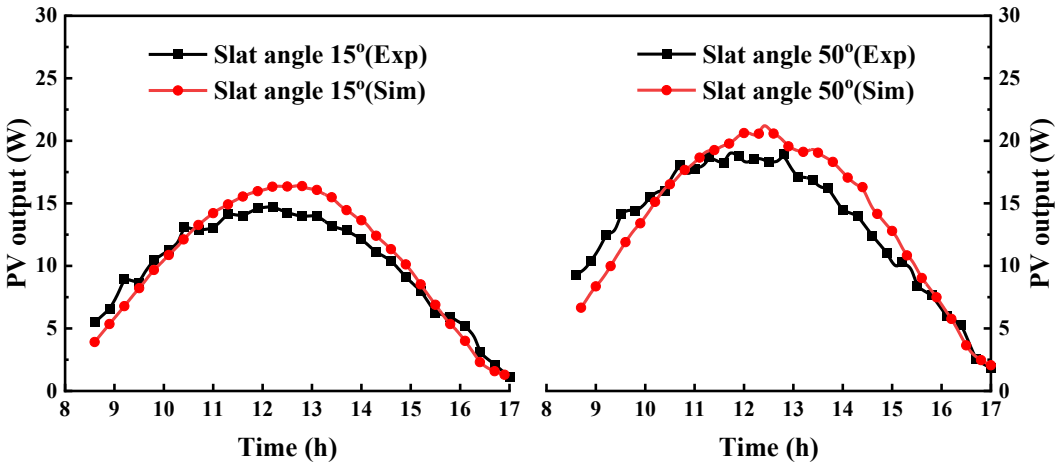

Fig. 10 The validation of the PV electricity model

4. Prediction methodology

In this study, an actual house with the office use characterized in our previous work [41] was used as the case to analyze the effect of the proposed windows on the overall energy performance of the building. The length, width and height of the building are 3.3 m, 3.1 m and 2.8 m respectively, and the proposed window with the dimensions of 3.15 m×1.2 m is applied on the south wall.

4.1. Climate conditions

Among the cities situated along the Yangtze River region, Shanghai (31.40 N, 121.45 E), Nanjing (32.83 N, 118.80 E), Wuhan (30.62 N, 114.13 E), and Chongqing (29.58 N, 106.47 E) were selected as the representative locations of upper, middle, and lower reaches, respectively. These cities

experience the subtropical humid climate and the climate characteristics are the Cfa (C: warm temperate, f: fully humid, a: hot summer) according to the Köppen-Geiger classification [63]. These regions are typically characterized by noticeable seasonal temperature variations. Winters are cold while summers are humid and hot. For the purposes of performance prediction, the weather data of typical meteorological year of these cities were utilized as boundary conditions for simulation. The meteorological information of these regions is provided in Table 1. Notably, the maximum and minimum temperatures experienced throughout the year range from 37℃ to 0℃, implying the presence of both heating and cooling demands in these regions. In these regions, the heating period is from Jan to Mar and from Nov to Dec while the cooling period is from May to Sep. The global horizontal irradiation (GHI) in these cities is between 1000 kWh/m^2 and 1450 kWh/m^2. According to the extended classification scheme of Skandalos et al. [64], the studied regions exhibit the medium level of GHI and belong to the moderate climate regions for PV integration. The analysis results of Skandalos et al. indicated that in the zones with medium GHI, it is feasible to achieve the positive energy buildings through combining PV roof, PV shadings, and PV wall façades [64].

Table 1 Meteorological information of the studied regions

	Köppen-Geiger classification	Maximum temperature (℃)	Minimum temperature (℃)	Global Horizontal Irradiation (kWh/m^2)
Shanghai	Cfa	36.8	-4.5	1443
Nanjing	Cfa	37.2	-5.6	1412
Wuhan	Cfa	38.8	-3.9	1349
Chongqing	Cfa	37.7	+2.8	1082

4.2. Parameter setting

In this study, the overall energy performance of the studied case, including power generation, air condition, artificial lighting, and water heating, was predicted based on the TRNSYS 18.0 platform. The component layout and data flow of the studied case in TRNSYS platform is shown in Fig. 11, and the corresponding parameter settings are shown in Table 2. The Type 56 was employed to model

the thermal balance of the building, and the physical properties of the wall material were inputted. According to the GB 19576-2019 in China, the rate performance coefficient for heating and cooling was assumed to be 4.0 and 3.0. The cooling and heating set temperatures were 24 ℃ and 20 ℃, respectively. The Type 158 was used to model the water tank for storing the hot water, and the gas boiler was modeled by Type 122 to heat the tank water to the desired temperature. According to the GB 50015-2019, the daily demand for hot water was 60 L/people and the desired temperature for water use was set to 45℃. The lighting electricity consumption was calculated using the Daylighting model in EnergyPlus software, which is a widely accepted and validated simulation tool [24]. According to the GB 50033-2013 in China, the artificial lighting density was 9 W/m^2 and the illuminance value setting was 500 lux. The lighting power obtained from the Daylighting model was imported into the Type 56 as the heat gain of the room. The mathematical models of the proposed window were programmed using the Matlab code, which was read by TRNSYS platform by the Type 155. The indoor heat gain and the water heat gain calculated by the Type 155 was inputted into the Type 56 and the Type 158 as the heat source. Meanwhile, the indoor temperature provides Type 56 and the water inlet temperature provided by the Type 158 was inputted to the Type 155 as the boundary condition. It was assumed that the water pump and fan are temperature-controlled. In the PV/water mode, the water pump is activated only when the temperature of the blind is higher than that of the tank. In the PV/air mode, the fan is activated only when the temperature of the cavity air is higher than that of the indoor air. The occupy time of the building, such as air condition, lighting, and water use, was set to 8:00~17:00. After above work was completed, the power generation from Type 155, the boiler power from Type 122, the lighting power from Energyplus, and air-conditioning power from Type 56 were integrated throughout the whole year.

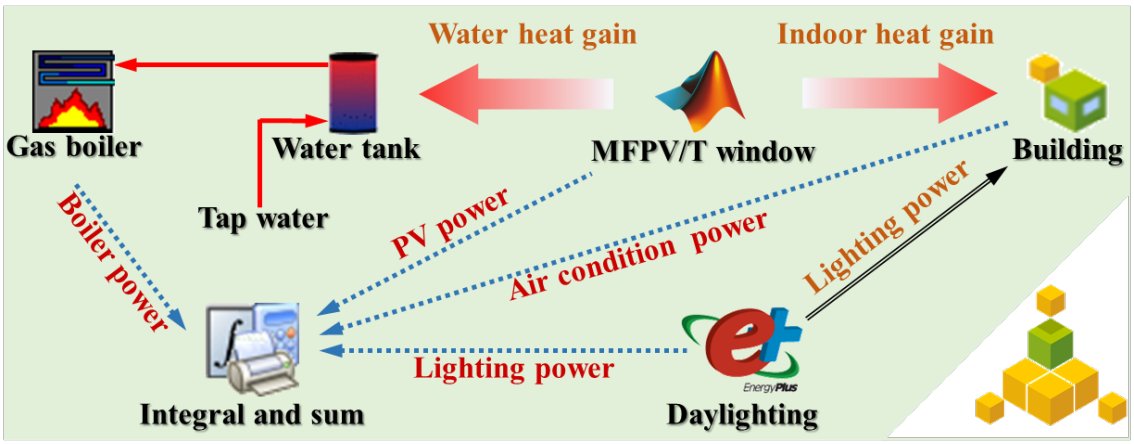

Fig. 11 The component layout and data flow of the studied case in TRNSYS platform

Table 2 The parameter setting of the studied case

Parameters		Value
MFPV/T window (Type 155)		
Outer glazing	Dimensions	3.15m (Width), 1.2m (High)
	Thickness	0.003 m
	Specific heat capacity	840 J/(kg·K)
	Density	2500 kg/m^3
	Transmittance	0.91
	Reflectance	0.08
	Emissivity	0.8
Inner glazing	Thickness	0.005 m
	Specific heat capacity	840 J/(kg·K)
	Density	2500 kg/m^3
	Transmittance	0.79
	Reflectance	0.073
	Emissivity	0.8
Air cavity	Depth	0.15 m
	Thickness	0.001 m
PV Blinds	Specific heat capacity	2750
	Density	
	Slat width	0.08 m
	Slat space	0.08 m
	Solar absorbance	0.9
	Emissivity	0.2
	Standard efficiency	0.17
	Temperature coefficient	0.0045 K^{-1}

	Inner diameter	0.007 m
	Thickness	0.001 m
Copper pipe	Specific heat capacity	385 J/(kg·K)
	Density	8933 kg/m^3
	Heat conductivity	397 W·m^{-2}·K^{-1}
Building (Type 56)		
	Dimensions	3.3m (Width), 2.8m (High)，3.1m (depth)
	Thickness	0.08m, 0.28m
Massive wall	Density	1st layer 15 kg/m^3, 2ed layer 1800 kg/m^3
	Specific heat capacity	1st layer 1.21 kJ/(kg·K), 2ed r layer 1.24 kJ/(kg·K)
	Heat conductivity	1st layer 0.18 W·m^{-2}·K^{-1}, 2ed layer 0.57 W·m^{-2}·K^{-1}
Water tank (Type 158)		
	Volume	0.12 m^3
	Height	1.3 m
	Number of nodes	3
	Loss coefficient	0.57 W·m^{-2}·K^{-1}
Gas boiler (Type 122)		
	Setpoint temperature	45℃
	Boiler efficiency	0.78
	Combustion efficiency	0.85
	Water flow rate	60 L/day
Daylighting (Energyplus)		
	Reference point of sensor	1.65 m (X), 1.55 m (Y), 1 m (Z)
	Artificial lighting density	9 W/m^2
	Lighting control type	continuous
	Illuminance setting value	500 lux

4.3. Performance evaluation

The impact of the proposed window on a building energy performance is assessed by PV electricity, air-conditioning load, artificial lighting, and domestic hot water. To comprehensively evaluate these aspects, this study employs the operation cost as the evaluation metric. In the Yangtze River region, the indoor air conditioning and artificial lighting are achieved by consuming the electricity from the grid while the gas boilers provide domestic hot water. Moreover, it is assumed that all PV output

generated by the proposed window is fed back into the grid. Therefore, the operation cost of the system can be calculated as:

$$C_{total} = \int (P_{AC}^{t} + P_{AL}^{t}) x_{ele} dt + \int x_{gas} \frac{Q_{boiler}^{t}}{HV \rho_{gas}} dt - \int P_{PV}^{t} x_{pv} dt \quad (56)$$

where, P_{AC}^{t}, P_{AL}^{t}, P_{PV}^{t}, and Q_{boiler}^{t} represent respectively air-conditioning power, lighting power, PV power, and gas boiler power. HV and ρ_{gas} are the heat value (55.627 MJ/kg) and density (0.716 kg/m^3) of the natural gas. x_{ele}, x_{pv}, and x_{gas} are the local grid electricity cost, PV feed-in tariff, and the price of natural gas per unit volume.

5. Results

5.1. Sensitivity analysis

This section aims to analyze the sensitivity of the proposed window's energy performance to variations in the slat angles, orientation, and type of inner glass. The default parameters considered in the analysis are a slat angle of 45^o, south orientation, and clear glass. The parameters are the same as the default parameters, except for the one discussed.

5.1.1. The impact of slat angle

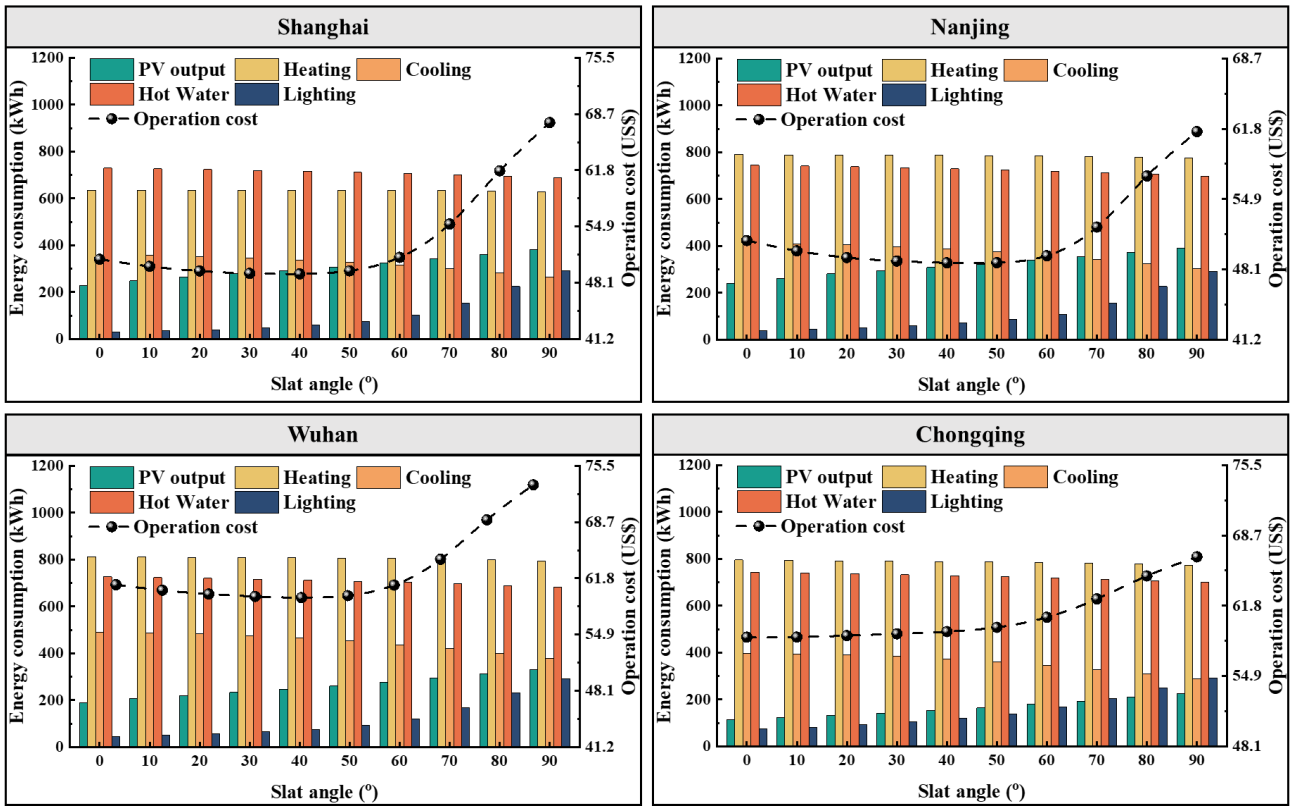

Fig. 12 Comparison of the proposed window with different slat angles

The comparison of the MFPV/T window with different slat angles is shown in Fig. 12. The trend of energy consumption and operation cost with the different blind angle is basically the same for the four cities. With an increase in slat angle, the PV out gradually increases while the energy consumption for heating water and air decreases. This suggests that an increase in the slat angle would enhance the solar energy utilization of the system, owing to reduced shading between the blinds. Moreover, increasing the blind angle also results in a reduction in the cooling load in summer, as less solar radiation enters the room. However, less visible light entering the room results in an increase in indoor lighting energy consumption. The annual operation cost of the studied case decreases firstly and then increases. The optimal slat angles for Shanghai, Nanjing, and Wuhan are 40~50° and that for Chongqing is 0°. The optimal angle in Chongqing is smaller in comparison to that in other cities, given the relatively lower irradiation in Chongqing, resulting in a larger proportion of lighting consumption. Therefore, ensuring indoor lighting is critical in Chongqing by decreasing the slat angle.

5.1.2. The impact of orientation

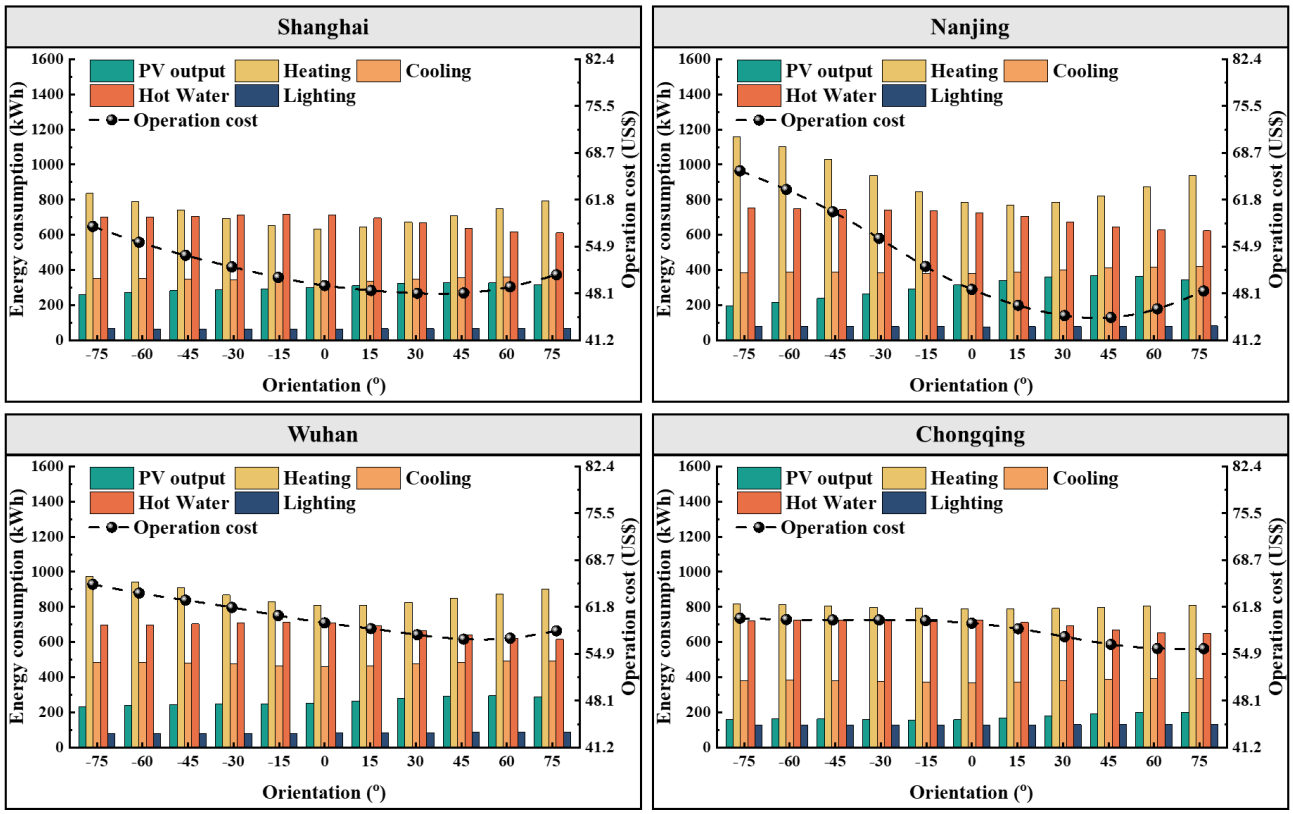

Fig. 13 Comparison of the proposed window with different orientation angles

The comparison of the MFPV/T window with different orientation angles is shown in Fig 13. It can be observed that the trends of the different types of energy consumption vary, owing to their distinct service periods. When the orientation angle is around 45~60°, the PV output is the largest. The minimum hot water load occurs when the orientation angle is 75°. The cooling and heating load reaches the minimum values when the orientation angle is 0°. The energy consumption for lighting remains almost the same for all orientations due to the 45° blind angle, which allows only diffuse radiation to enter the room, and is almost uniform for all orientations. After weighted summation, the optimal orientation angles for Shanghai, Nanjing, Wuhan, and Chongqing are 30°, 45°, 45°, and 60°.

5.1.3. The impact of inner glass

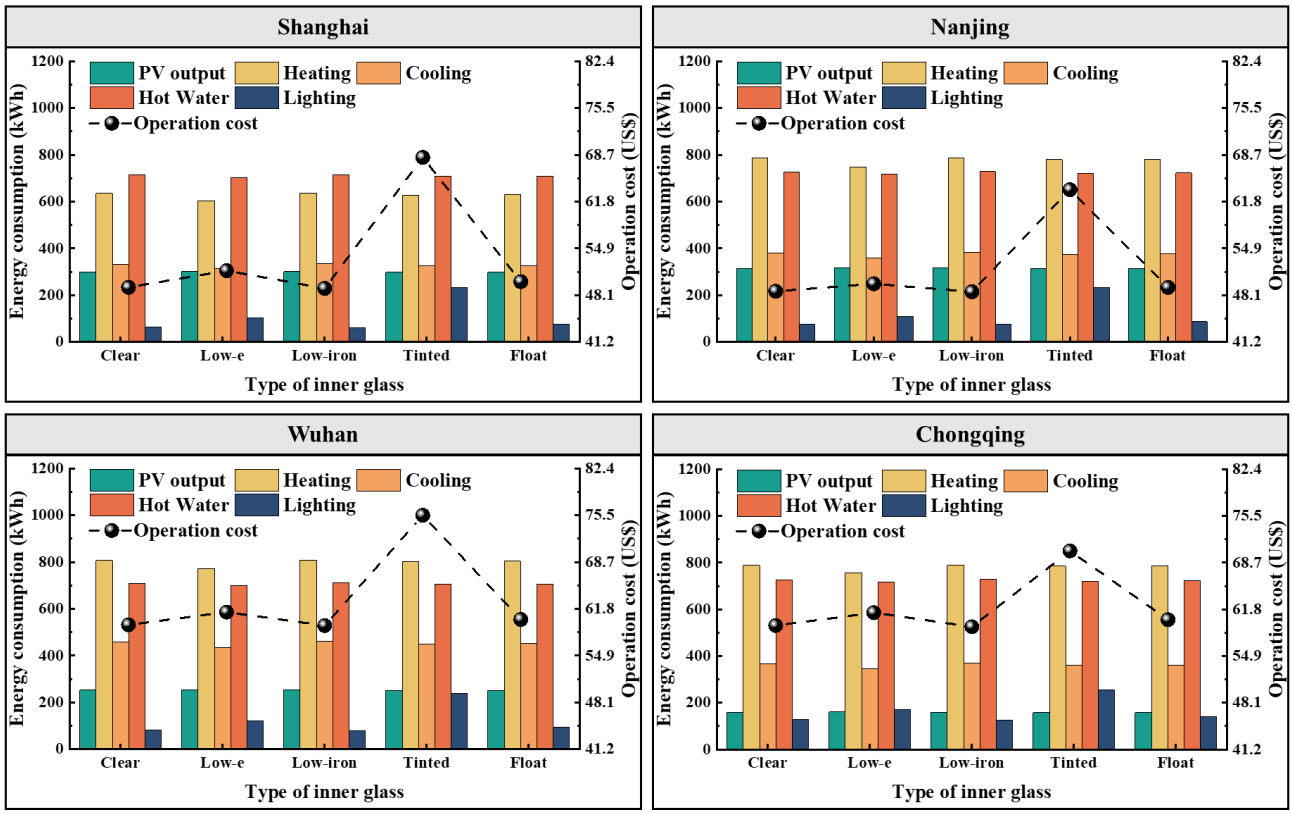

Fig. 14 Comparison of the proposed window with different inner glasses

The comparison of the MFPV/T window with different inner glasses is shown in Fig. 14. The analyzed inner glass types, besides clear glass, include low-e glass, low-iron glass, tinted glass, and float glass. The corresponding data of optical properties are acquired from the International Glazing Database (IGDB) [65]. The results indicate that the impact of inner glazing on energy consumption is consistent across all four cities. The proposed window with low-e glass has the best performance in terms of PV output, air conditioning load, and hot water load. Apart from low-e glass, the proposed window with tinted glass has lower heating and cooling loads compared to other types of inner glass. It can be observed that increasing the solar absorbance of the inner glass helps to reduce the energy consumption of air conditioning. However, the low visible transmittance of low-e and tinted glass increases the lighting consumption, resulting in higher operating costs. Based on the weighted sum of all energy consumption, the proposed window with low-iron glass has the lowest operation cost among all tested inner glass types.

5.2. Energy saving potential of proposed system

In this section, a detailed analysis of the energy performance of the proposed system is presented. In the Yangtze region, the double-skin clear window is commonly used in office buildings, so it was chosen as a reference to evaluate the energy-saving potential of the proposed system. The slat angle and inner glass of the MFPV/T window are the optimized results in the previous section and the building orientation is assumed to be south.

5.2.1. Power generation

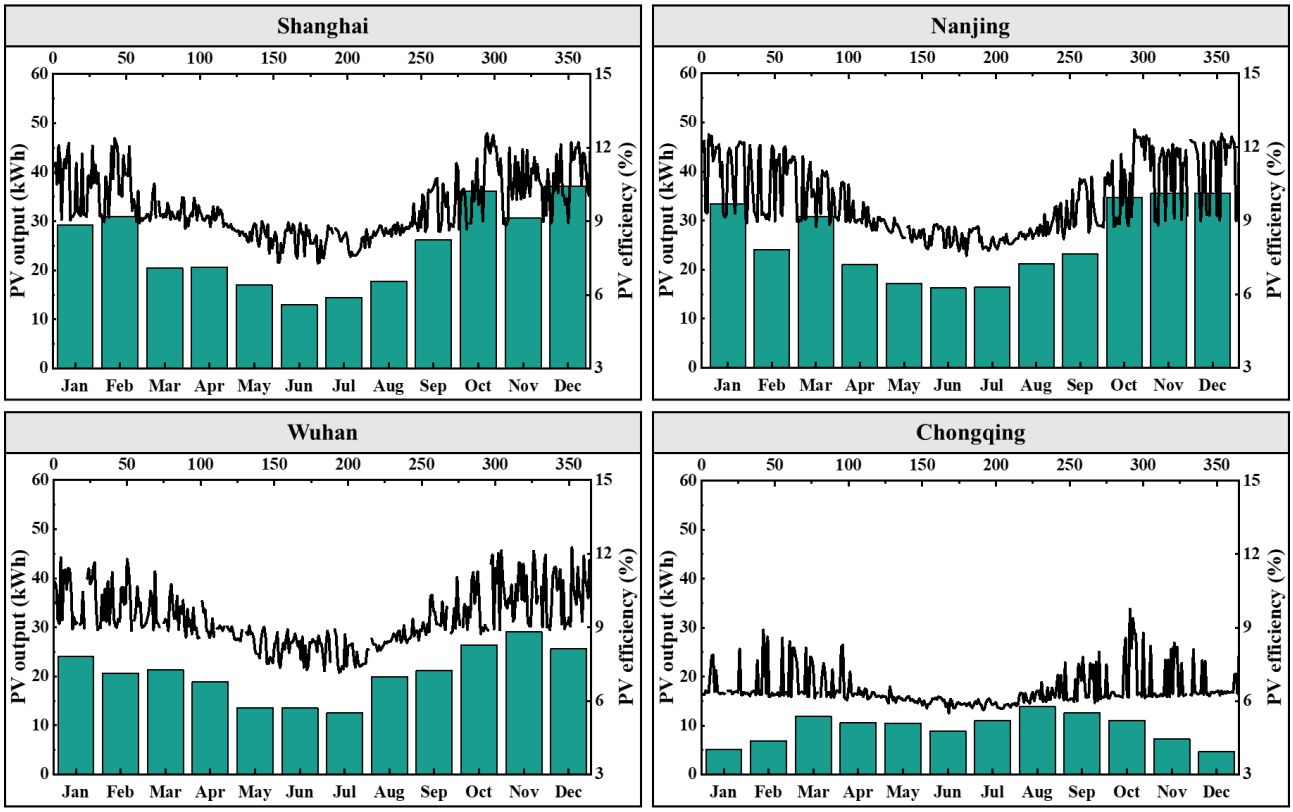

Fig. 15 Monthly PV output and daily PV efficiency of the proposed window

The monthly PV output and daily PV efficiency of the proposed window throughout the whole year is shown in Fig. 15. The PV efficiency is defined as the ratio of the power generation to the total irradiation on the outer glazing. The PV output mainly depends on the irradiation. In Shanghai, Nanjing, and Wuhan, the maximum monthly PV output occurs between Nov to Dec. Overall, the

trend of monthly PV output in these areas is high in winter and low in summer. Conversely, in Chongqing, the monthly PV output is lower due to the rainy weather and the maximum monthly PV output occurs on Aug. The annual PV outputs in these four cities are 77.6 kWh/m^2, 82.4 kWh/m^2, 65.8 kWh/m^2, and 30.2 kWh/m^2, respectively. The daily PV efficiency varies dramatically and is impacted by many factors. Only a small portion of the diffuse irradiation hits the front side of the blinds due to the view factor. Hence, the PV efficiency on cloudy day is lower than that on sunny day. Furthermore, the shading between the blinds is less pronounced at low solar altitude angles, leading to higher efficiency in winter than in summer. The average PV efficiencies during the whole year in these four cities are 10.0%, 10.4%, 9.8%, and 6.7%, respectively.

5.2.2. Air-conditioning load

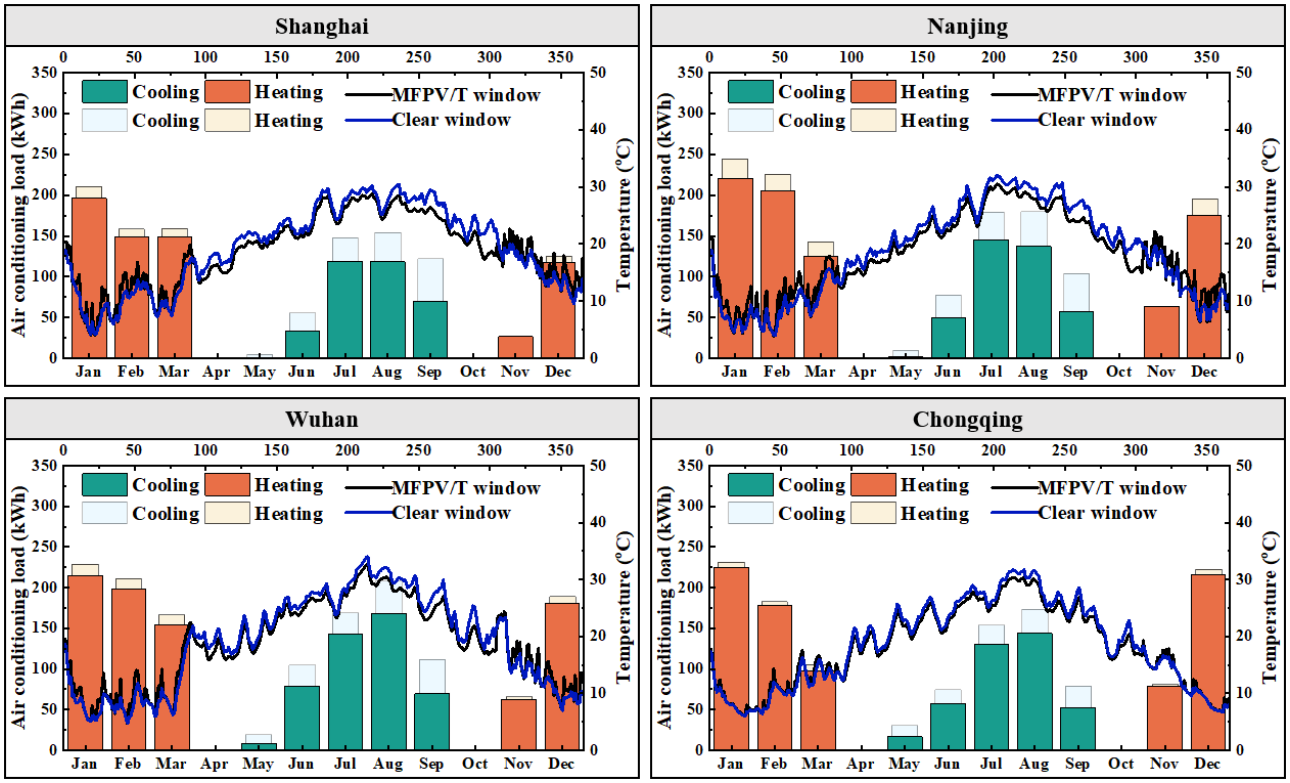

Fig. 16 Comparison of monthly air conditioning load and daily average indoor temperature

The comparison of monthly air conditioning load and daily average indoor temperature between MFPV/T and clear windows is shown in Fig. 16. Compared with the clear window, the MFPV/T window can reduce both the winter heating load and the summer cooling load. In summer, the shading

of the blind reduces the irradiation entering to the room, while the cooling of water pipe can reduce the convention heat gain from the window. As a result, the cooling load is reduced significantly. In winter, the heating load is also reduced, which can be attributed to two main factors. Firstly, the blinds enhance the thermal insulation performance of the proposed system. This improved thermal insulation performance leads to better heat retention within the indoor space, resulting in a decreased heating demand. Secondly, while the amount of irradiation entering the room is reduced, a portion of it is absorbed by the blinds and converted into convective heat gain. This convective heat gain in the room air promptly contributes to a temperature rise, thereby reducing the heating load during operational hours. Compared with the clear window, the MFPV/T window can reduce the air conditioning load by 15.4%, 16.8%, 13.1%, and 10.2% in Shanghai, Nanjing, Wuhan, and Chongqing, respectively. The heating and cooling functions of the proposed window can also be found from the comparison of daily average indoor temperature when the air conditioner is turned off. The indoor temperature is increased in winter and decreased in summer. The average temperature difference is around 3℃.

5.2.3. Hot water supplement

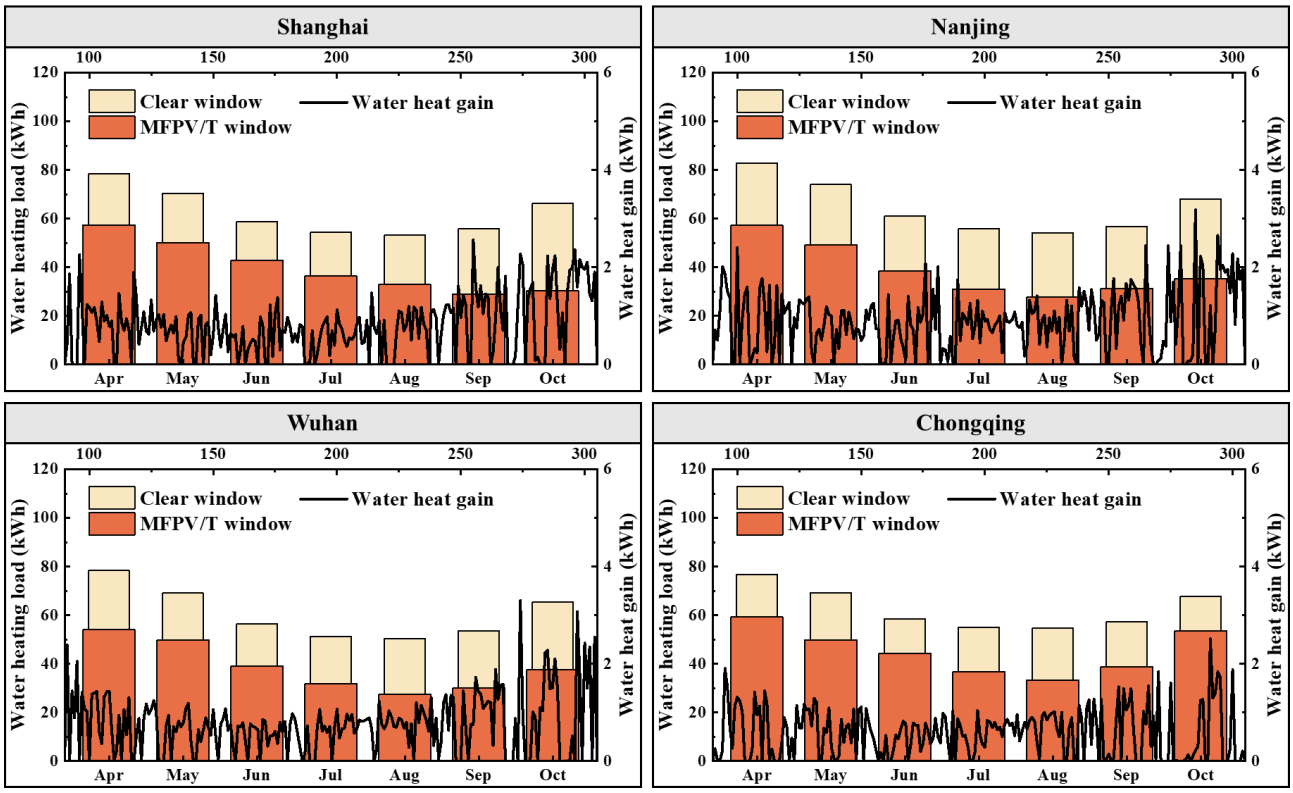

Fig. 17 Comparison of monthly water heating load and daily water heat gain

The comparison of monthly water heating load and daily water heat gain between MFPV/T and clear windows is shown in Fig. 17. Since the proposed system provides hot water only during the non-heating seasons, the water heating load in the heating seasons is not analyzed in this subsection. It is observed that the monthly water heating load varies with the month, which can be attributed to the variation in tap water temperature throughout the year. Specifically, the water heating load in summer is lower than that in other seasons. Compared with the clear window, the water heating load of the MFPV/T window is decreased significantly because the water is pre-heated by the proposed window. The monthly reduction of water-heating load is around 20 kWh. After summing, the annual energy savings for water heating are 41.8 kWh/m^2, 48.4 kWh/m^2, 40.7 kWh/m^2, and 32.5 kWh/m^2, respectively. Furthermore, the daily water heat gain of the proposed window is around 0.47 kWh, 0.52 kWh, 0.44 kWh, and 0.33 kWh in these four cities. The water heat gain in the transition season is higher than that in summer due to changes in irradiation. In individual rainy days, the daily water heat gain is zero as the pump is always off.

5.2.4. Daylighting performance

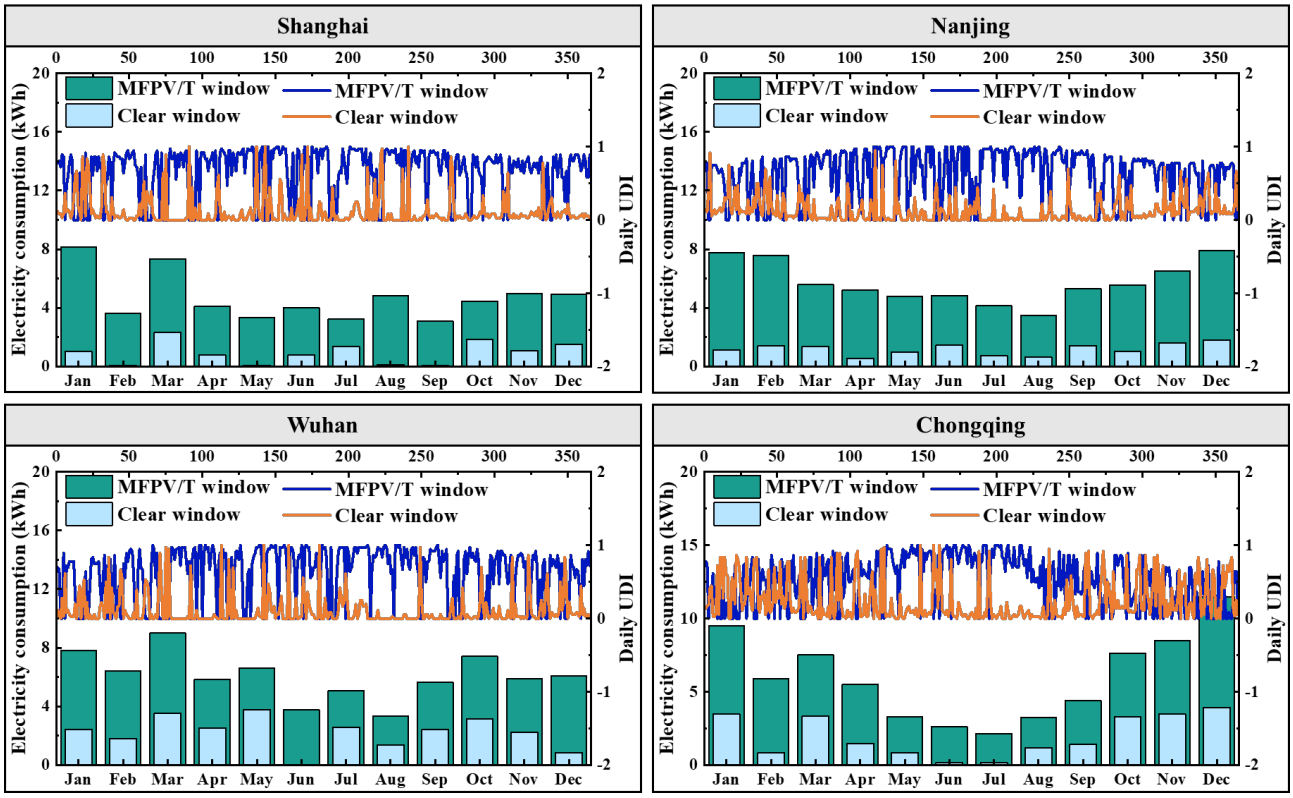

Fig. 18 Comparison of monthly lighting electricity consumption load and daily UDIs

The comparison of monthly water heating load and daily water heat gain between MFPV/T and clear windows is shown in Fig. 18. The lighting consumption of the MFPV/T window is consistently higher than that of the clear window due to the shading of the PV blind. The annul lighting consumptions of the MFPV/T windows are 56.0 kWh, 68.7 kWh, 73.0 kWh, and 71.7 kWh while these of clear window are 11.1 kWh, 14.2 kWh, 26.8 kWh, and 23.6 kWh. Although the lighting energy consumption of clear windows is low, excessive indoor illuminance may cause human visual discomfort. The useful daylight illuminance (UDI) is a widely used metric for evaluating the daylighting performance of the window, which is defined as the percentage of the work time that the work plane illuminance falls within the desired ranges [6]. The upper limit of daylighting is usually 2000 lux because the visual discomfort such as glare may occur when the illuminance exceeds this value. Considering the low limit of daylighting is 500 lux in this study, the desired ranges for UDI is 500~2000 lux. From the profiles in Fig. 18, it can be observed that the UDI of MFPV/T window is

larger than that of clear window for most of the year (especially in summer). After summing, the time that the illuminance value is within the desired range for MFPV/T window is higher than that for clear window by approximately 53%, 51%, 50%, and 25% in the respective cities.

5.2.5. Overall energy saving

After analyzing the monthly and daily electrical, thermal, and daylighting performance of the proposed window, it is evident that the window has significant energy-saving potential in the Yangtze River region. The overall energy savings achieved by the MFPV/T window are summarized and listed in Table 3. The energy benefits of the MFPV/T window include PV output, cooling, heating, and hot water supplement. Additionally, the proposed window provides better human visual comfort at the cost of additional artificial lighting consumption. In the case study, the annual energy costs for these four cities are reduced by 34%, 36%, 28%, and 16% when compared to the double-skin clear window. This reduction translates to economic benefits of 6.4 \$/m^2, 7.0 \$/m^2, 5.7 \$/m^2, and 2.9 \$/m^2 throughout the year. The proposed system leads to the generation of PV electricity and savings in air conditioner electricity consumption, resulting in reduced CO_2 emissions when compared to the double-skin clear window. Additionally, the decreased consumption of natural gas in the gas boiler also contributes to a reduction in CO_2 emissions. In this section, the reduction in CO_2 emissions achieved by the MFPV/T window system is quantified. In China, the equivalent CO_2 emissions per unit of grid electricity consumption is 0.572 kg/kWh and the CO_2 produced by the combustion of a unit mass of natural gas is 2.75 kg/kg [66]. For the studied case, the annual CO_2 emission reduction due to the energy saving of the MFPV/T window system is estimated at 53.5 kg/m^2, 58.5 kg/m^2, 47 kg/m^2, and 22.3 kg/m^2 for the respective cities studied. It should be noted that if more efficient air conditioning and lighting devices are used, the energy savings potential of the proposed window will be even greater.

Table 3 The energy savings of the MFPV/T window during the whole year (kWh)

	PV output	Cooling	Heating	Hot water	Lighting
Shanghai	293.4	142.2	35.2	158.0	-44.9
Nanjing	309.3	158.3	79.7	182.6	-54.5

Wuhan	246.9	143.7	49.1	154.9	-46.2
Chongqing	114.2	110.4	25.2	123.3	-48.1

6. Discussion

The preceding section provided an overview of the system's influence on diverse energy consumption aspects. Nevertheless, it's imperative to acknowledge that the findings of this investigation are specific to the examined cases. The results of sensitivity analysis and energy savings are related to the factors such as building layout, wall compositions, window dimensions, energy consumption patterns, and the efficiency of the building energy equipment. The outlined case studies were devised to uncover the patterns in the proposed system's impact on the diverse energy aspects of the building. In this section, the system's application prospective and the potential barriers are discussed.

In terms of building types, the proposed system exhibits suitability not only for office buildings but also for residential and commercial buildings. The latter two categories maintain significant water-heating requirements alongside their air conditioning and electricity loads. Nevertheless, the capacity configurations of the system across different building types must be tailored according to their distinct energy demands. For instance, commercial establishments like restaurants tend to necessitate more hot water, making a larger deployment of the proposed system viable. Conversely, the office and residential buildings typically entail less water consumption. Excessive installation of MFPV/T windows might compromise the water heating efficiency for the proposed system. In terms of application positioning, the system finds applicability in windows, curtain walls, skylights, and other fenestration structures. When deploying it in diverse locations, the careful consideration is warranted while determining the blind angles for optimizing solar irradiation collection while ensuring adequate indoor daylighting effects. In terms of economics, the system's primary components encompass glasses, PV cells, copper tubes, and aluminum slats. These materials are both economical and widely accessible, implying that the system's material cost remains low and affordable. Moreover, as the cost of PV cells continues to decline, the overall market price of the proposed system is anticipated to further decrease. Therefore, it can be reasonably deduced that the

affordability of the proposed system would be attainable upon market adoption. Furthermore, the simple construction of the MFPV/T window allows its dimensions to be easily customized, including the length and number of the PV/T blinds. This adaptability empowers users to select the system capacity that aligns with their budget and the energy demand of the building.

However, it's important to recognize that the proposed system is designed to supplement the building's traditional HVAC (Heating, Ventilation, and Air Conditioning) systems, rather than serve as its primary energy source. The main reasons are as following:

- Limited energy cost reduction: In the cases studied, the installation of the proposed windows reduced the annual energy costs of the houses studied by only 16~36%. It's important to note that the studied case pertains to a small office with minimal energy consumption. For the larger buildings, the reduction rate will be even lower.
- Dependence on solar energy: The MFPV/T system primarily relies on solar energy and functions exclusively during daylight hours. This renders its utility limited during nighttime and overcast periods. Even with the integration of energy storage, the solar energy on south facade in the Yangtze River region remains almost inadequate for comprehensive building energy coverage.
- Seasonal Limitations: The water heating function of the MFPV/T window is active only during the non-heating seasons. This poses limitations since the hot water demand exists across various seasons.

While the proposed system offers the multifaceted energy benefits due to its seasonal adaptability, several barriers still exist for future market uptake:

- Reliability: The proposed system's primary application positions are fenestrations, demanding robust protection against rain, snow, and safety concerns, especially in high-rise buildings. Moreover, the PV/T blinds constitute the core of the proposed system. Yet, the challenge of ensuring the durability of the lamination process between PV modules and heat-absorbing slats, a longstanding hurdle in the marketability of PV/T modules, remains for the proposed system.
- Standardization: The diversity in building fenestrations, encompassing various shapes, sizes, and wall thicknesses, poses challenges for customization on a per-building basis by manufacturers. To facilitate practical implementation, the development of standardized product norms of MFPV/T

window that cater to the requirements of building-integrated PV and solar collector industries is crucial.

- Refurbishment: Integrating the MFPV/T window into existing buildings can be complex. It involves not only replacing the building's original glazing system but also adapting the proposed system to fit. Moreover, connecting the system's header pipes to the building's water heating system adds to the intricacy of retrofitting.

Overall, the concept of the MFPV/T window is first proposed in this study. By amalgamating PV/T technology with a building's external windows, the system effectively mitigates space heating, space cooling, and water heating loads while generating clean electricity and enhancing visual comfort. This system's implementation holds the potential to propel existing buildings towards zero-energy or even positive-energy status in regions characterized by hot summers and cold winters. In the future work, the authors will fabricate a prototype of the MFPV/T window based on the insights garnered from this study. Moreover, an assessment of the system's energy efficiency across diverse building types, alongside quantifying its potential contribution to greenhouse gas reduction in the short and medium term, will be pursued. Additionally, an in-depth economic analysis of the system will be undertaken, encompassing all aspects of its preparation and utilization.

7. Conclusion

In this study, a novel multi-functional PV/T window was proposed to enhance the solar energy utilization and seasonal adaptability. This window features a PV blind positioned within the cavity of a double-skin ventilation window, with water pipes welded behind the PV blind. In winter, the cavity air exchanges with the indoor air, allowing heat on the PV blind to be recovered to increase the indoor temperature. In summer and other seasons, the tank water is induced into the water pipe for cooling, thereby reducing indoor heat gain, while the heat on the PV blind is recovered to produce hot water. By switching between different work modes according to the season, the proposed window enables comprehensive solar utilization of photovoltaic and photothermal energy throughout the year. To evaluate the energy saving potential of the proposed system, the mathematical model of the proposed

window was built and validated by the reported data. Then, the developed model was integrated into TRNSYS platform to calculate the electrical and thermal performance, while the EnergyPlus software was used to calculate the daylighting performance. Using these methodologies, the overall energy consumption of the MFPV/T window was predicted and analyzed based on the weather data of Yangtze River region: Shanghai, Nanjing, Wuhan, and Chongqing. Firstly, the sensitivity analysis of slat angle, orientation, and inner glass of the proposed window system was analyzed. Then, the annual energy consumption and operation cost of the buildings installed with MFPV/T and clear windows were compared. The main results are summarized as follows:

(1) Increasing the slat angle can increase the heat and electrical output of the system, but it can also increase the lighting energy consumption. The optimal slat angles for Shanghai, Nanjing, and Wuhan are 40°, while for Chongqing it is 0°. The PV output, air conditioning load, and hot water production reach the optimal value when the orientation angles are 45~60°, 0°, and 75°, respectively. The orientation angle has negligible effect on the lighting energy consumption of the proposed system. The optimal orientation angles for these cities are 30°, 45°, 45°, and 60°, respectively. Due to the shading of the PV blind, low-iron glass with high visual penetration is preferred as the inner glass over low-emissivity glass with insulation properties.

(2) The annual PV outputs in these four cities are 77.6 kWh/m^2, 82.4 kWh/m^2, 65.8 kWh/m^2, and 30.2 kWh/m^2, respectively. Compared with the double-skin clear window, the MFPV/T window can reduce the air conditioning load by 15.4%, 16.8%, 13.1%, and 10.2%, respectively, while the water heating loads are reduced by 41.8 kWh/m^2, 48.4 kWh/m^2, 40.7 kWh/m^2, and 32.6 kWh/m^2, respectively. Additionally, the UDIs are increased by around 53%, 51%, 50%, and 25%, at the cost of an increase in lighting consumption of 11.9 kWh/m^2, 14.4 kWh/m^2, 12.2 kWh/m^2 and 12.7 kWh/m^2, respectively. After using the MFPV/T window, the operation cost during the whole year can be reduced by 34% (6.4 \$/m^2), 36% (7.0 \$/m^2), 28% (5.7 \$/m^2), and 16% (2.9 \$/m^2), respectively while the CO_2 emission can be reduced by 53.5, 58.5, 47, and 22.3 kg/m^2, respectively.

Acknowledgement

This work was supported by the research funding of the Joint Postdoc Scheme with Non-local Institutions of The Hong Kong Polytechnic University.

Reference

[1] Pan W, Teng Y. A systematic investigation into the methodological variables of embodied carbon assessment of buildings. Renewable and Sustainable Energy Reviews. 2021;141.

[2] Christopher S, Vikram MP, Bakli C, Thakur AK, Ma Y, Ma Z, et al. Renewable energy potential towards attainment of net-zero energy buildings status – A critical review. Journal of Cleaner Production. 2023;405.

[3] Windows Key to Increased Energy Efficiency in Buildings and Achieving Clean Energy Economy. U.S. Department of Energy. Available online: www.energy.gov/eere/buildings. [Accessed 2 April 2023].

[4] Uddin MM, Jie J, Wang C, Zhang C, Ke W. A review on photovoltaic combined vacuum glazing: Recent advancement and prospects. Energy and Buildings. 2023;286.

[5] Skandalos N, Karamanis D. PV glazing technologies. Renewable and Sustainable Energy Reviews. 2015;49:306-22.

[6] Wang C, Ji J, Yu B, Zhang C, Ke W, Wang J. Comprehensive investigation on the luminous and energy-saving performance of the double-skin ventilated window integrated with CdTe cells. Energy. 2022;238.

[7] Su X, Zhang L, Luo Y, Liu Z, Yang H, Wang X. Conceptualization and preliminary analysis of a novel reversible photovoltaic window. Energy Conversion and Management. 2021;250.

[8] Olivieri L, Caamaño-Martin E, Olivieri F, Neila J. Integral energy performance characterization of semi-transparent photovoltaic elements for building integration under real operation conditions. Energy and Buildings. 2014;68:280-91.

[9] Skandalos N, Karamanis D. Investigation of thermal performance of semi-transparent PV technologies. Energy and Buildings. 2016;124:19-34.

[10] Alrashidi H, Ghosh A, Issa W, Sellami N, Sundaram SJSE. Thermal performance of semitransparent CdTe BIPV window at temperate climate. 2020;195:536-43.

[11] Lee HM, Yoon JH. Power performance analysis of a transparent DSSC BIPV window based on 2 year measurement data in a full-scale mock-up. Applied Energy. 2018;225:1013-21.

[12] Lu L, Law KM. Overall energy performance of semi-transparent single-glazed photovoltaic (PV) window for a typical office in Hong Kong. Renewable Energy. 2013;49:250-4.

[13] Fung TYY, Yang H. Study on thermal performance of semi-transparent building-integrated photovoltaic glazings. Energy and Buildings. 2008;40:341-50.

[14] Liao W, Xu S. Energy performance comparison among see-through amorphous-silicon PV (photovoltaic) glazings and traditional glazings under different architectural conditions in China. Energy. 2015;83:267-75.

[15] Wang M, Peng J, Li N, Yang H, Wang C, Li X, et al. Comparison of energy performance between PV double skin facades and PV insulating glass units. Applied Energy. 2017;194:148-60.

[16] Park KE, Kang GH, Kim HI, Yu GJ, Kim JT. Analysis of thermal and electrical performance of semi-transparent photovoltaic (PV) module. Energy. 2010;35:2681-7.

[17] Peng J, Lu L, Yang H, Ma T. Validation of the Sandia model with indoor and outdoor measurements for semi-transparent amorphous silicon PV modules. Renewable Energy. 2015;80:316-23.
[18] Song J-H, An Y-S, Kim S-G, Lee S-J, Yoon J-H, Choung Y-K. Power output analysis of transparent thin-film module in building integrated photovoltaic system (BIPV). Energy and Buildings. 2008;40:2067-75.
[19] Han J, Lu L, Peng J, Yang H. Performance of ventilated double-sided PV façade compared with conventional clear glass façade. Energy and Buildings. 2013;56:204-9.
[20] Han J, Lu L, Yang H. Thermal behavior of a novel type see-through glazing system with integrated PV cells. Building and Environment. 2009;44:2129-36.
[21] Chen F, Wittkopf SK, Khai Ng P, Du H. Solar heat gain coefficient measurement of semi-transparent photovoltaic modules with indoor calorimetric hot box and solar simulator. Energy and Buildings. 2012;53:74-84.
[22] Liu D, Sun Y, Wilson R, Wu Y. Comprehensive evaluation of window-integrated semi-transparent PV for building daylight performance. Renewable Energy. 2020;145:1399-411.
[23] Kapsis K, Dermardiros V, Athienitis AKJEP. Daylight Performance of Perimeter Office Façades utilizing Semi-transparent Photovoltaic Windows: A Simulation Study. 2015;78:334-9.
[24] Wang M, Peng J, Li N, Lu L, Ma T, Yang H. Assessment of energy performance of semi-transparent PV insulating glass units using a validated simulation model. Energy. 2016;112:538-48.
[25] Chen M, Zhang W, Xie L, Ni Z, Wei Q, Wang W, et al. Experimental and numerical evaluation of the crystalline silicon PV window under the climatic conditions in southwest China. Energy. 2019;183:584-98.
[26] Sun Y, Shanks K, Baig H, Zhang W, Hao X, Li Y, et al. Integrated semi-transparent cadmium telluride photovoltaic glazing into windows: Energy and daylight performance for different architecture designs. Applied Energy. 2018;231:972-84.
[27] Qiu C, Yang H. Daylighting and overall energy performance of a novel semi-transparent photovoltaic vacuum glazing in different climate zones. Applied Energy. 2020;276.
[28] Ghosh A, Sundaram S, Mallick TK. Investigation of thermal and electrical performances of a combined semi-transparent PV-vacuum glazing. Applied Energy. 2018;228:1591-600.
[29] Ghosh A, Sarmah N, Sundaram S, Mallick TK. Numerical studies of thermal comfort for semi-transparent building integrated photovoltaic (BIPV)-vacuum glazing system. Solar Energy. 2019;190:608-16.
[30] Ghosh A, Sundaram S, Mallick TK. Colour properties and glazing factors evaluation of multicrystalline based semi-transparent Photovoltaic-vacuum glazing for BIPV application. Renewable Energy. 2019;131:730-6.
[31] Uddin MM, Wang C, Zhang C, Ji J. Investigating the energy-saving performance of a CdTe-based semi-transparent photovoltaic combined hybrid vacuum glazing window system. Energy. 2022;253.
[32] Luo Y, Zhang L, Liu Z, Xie L, Wang X, Wu J. Experimental study and performance evaluation of a PV-blind embedded double skin façade in winter season. Energy. 2018;165:326-42.
[33] Kang S, Hwang T, Kim JT. Theoretical analysis of the blinds integrated photovoltaic modules. Energy and Buildings. 2012;46:86-91.
[34] Gao Y, Dong J, Isabella O, Santbergen R, Tan H, Zeman M, et al. A photovoltaic window with sun-tracking shading elements towards maximum power generation and non-glare daylighting. Applied Energy. 2018;228:1454-72.
[35] Hong S, Choi A-S, Sung M. Development and verification of a slat control method for a bi-directional PV blind. Applied Energy. 2017;206:1321-33.
[36] Hong S, Choi A, Sung M. Impact of bi-directional PV blind control method on lighting, heating and cooling energy consumption in mock-up rooms. Energy and Buildings. 2018;176:1-16.

[37] Yu G, Yang H, Luo D, Cheng X, Ansah MK. A review on developments and researches of building integrated photovoltaic (BIPV) windows and shading blinds. Renewable and Sustainable Energy Reviews. 2021;149.
[38] Peng J, Lu L, Yang H. An experimental study of the thermal performance of a novel photovoltaic double-skin facade in Hong Kong. Solar Energy. 2013;97:293-304.
[39] Luo Y, Zhang L, Liu Z, Su X, Lian J, Luo Y. Coupled thermal-electrical-optical analysis of a photovoltaic-blind integrated glazing façade. Applied Energy. 2018;228:1870-86.
[40] Chialastri A, Isaacson M. Performance and optimization of a BIPV/T solar air collector for building fenestration applications. Energy and Buildings. 2017;150:200-10.
[41] Wang C, Ji J, Uddin MM, Yu B, Song Z. The study of a double-skin ventilated window integrated with CdTe cells in a rural building. Energy. 2021;215.
[42] Jia J, Gao F, Cheng Y, Wang P, Ei-Ghetany HH, Han J. A comparative study on thermoelectric performances and energy savings of double-skin photovoltaic windows in cold regions of China. Solar Energy. 2020;206:464-72.
[43] Su X, Zhang L, Luo Y, Liu Z. Energy performance of a reversible window integrated with photovoltaic blinds in Harbin. Building and Environment. 2022;213.
[44] Wang Y, Chen Y, Li C. Energy performance and applicability of naturally ventilated double skin façade with Venetian blinds in Yangtze River Area. Sustainable Cities and Society. 2020;61.
[45] China Building Energy Research Report (2022). CABEE. 2022.
[46] Wang M, Wang Y, Wu Y, Yue X, Wang M, Hu P. Identifying the spatial heterogeneity in the effects of the construction land scale on carbon emissions: Case study of the Yangtze River Economic Belt, China. Environ Res. 2022;212:113397.
[47] Guo W, Kong L, Chow T, Li C, Zhu Q, Qiu Z, et al. Energy performance of photovoltaic (PV) windows under typical climates of China in terms of transmittance and orientation. Energy. 2020;213.
[48] Pfrommer P, Lomas KJ, Kupke CJSE. Solar radiation transport through slat-type blinds: A new model and its application for thermal simulation of buildings. 1996;57:77-91.
[49] Beckman. JADWA. Solar Engineering of Thermal Processes. University of Wisconsin-Madison1980.
[50] Zanghirella F, Perino M, Serra V. A numerical model to evaluate the thermal behaviour of active transparent façades. Energy and Buildings. 2011;43:1123-38.
[51] Wang Y, Chen Y. Modeling and calculation of solar gains through multi-glazing facades with specular reflection of venetian blind. Solar Energy. 2016;130:33-45.
[52] Xu L, Luo K, Ji J, Yu B, Li Z, Huang S. Study of a hybrid BIPV/T solar wall system. Energy. 2020;193.
[53] Handbook AF. American society of heating, refrigerating and air-conditioning engineers. Inc: Atlanta, GA, USA. 2009.
[54] Khalvati F, Omidvar A. Summer study on thermal performance of an exhausting airflow window in evaporatively-cooled buildings. Applied Thermal Engineering. 2019;153:147-58.
[55] ISO 15099, Thermal performance of windows, doors and shading devices — Detailed calculations. 2003.
[56] Jiru TE, Haghighat F. Modeling ventilated double skin façade—A zonal approach. Energy and Buildings. 2008;40:1567-76.
[57] Lienhard JH. A heat transfer textbook: Phlogistron; 2005.
[58] ASHRAE AG. Guideline 14-2014: Measurement of energy, demand, and water savings. American Society of Heating, Refrigerating, and Air Conditioning Engineers, Atlanta, Georgia. 2014.
[59] Luo Y, Zhang L, Wu J, Wang X, Liu Z, Wu Z. Modeling of solar transmission through multilayer glazing facade

using shading blinds with arbitrary geometrical and surface optical properties. Energy. 2017;128:163-82.
[60] Zhang C, Gang W, Wang J, Xu X, Du Q. Experimental investigation and dynamic modeling of a triple-glazed exhaust air window with built-in venetian blinds in the cooling season. Applied Thermal Engineering. 2018;140:73-85.
[61] Yan S, Li X, Wang B, Shi W, Lyu W. A method to describe the thermal property of pipe-embedded double-skin façade: Equivalent glass window. Energy and Buildings. 2019;195:33-44.
[62] Hu Z, He W, Hu D, Lv S, Wang L, Ji J, et al. Design, construction and performance testing of a PV blind-integrated Trombe wall module. Applied Energy. 2017;203:643-56.
[63] Beck HE, Zimmermann NE, McVicar TR, Vergopolan N, Berg A, Wood EF. Present and future Köppen-Geiger climate classification maps at 1-km resolution. Scientific data. 2018;5:1-12.
[64] Skandalos N, Wang M, Kapsalis V, D'Agostino D, Parker D, Bhuvad SS, et al. Building PV integration according to regional climate conditions: BIPV regional adaptability extending Köppen-Geiger climate classification against urban and climate-related temperature increases. Renewable and Sustainable Energy Reviews. 2022;169.
[65] Laboratory LBN. International Glazing Database. Available online: https://windowslblgov/software/igdb. [Accessed 2 December 2022].
[66] Wang C, Ji J. Comprehensive performance analysis of a rural building integrated PV/T wall in hot summer and cold winter region. Energy. 2023.